JOURNAL OF GEOPHYSICAL RESEARCH, VOL. 86, NO. A10, PAGES 8259–8284, SEPTEMBER 30, 1981

Overview of the Voyager Ultraviolet Spectrometry Results Through Jupiter Encounter

A. L. BROADFOOT,[1] B. R. SANDEL,[1] D. E. SHEMANSKY,[1] J. C. MCCONNELL,[1,5] G. R. SMITH,[1] J. B. HOLBERG,[1] S. K. ATREYA,[2] T. M. DONAHUE,[2] D. F. STROBEL,[3] AND J. L. BERTAUX[4]

The Voyager ultraviolet spectrometers (UVS) have been making almost continuous observations, in the 500-Å to 1700-Å wavelength range, of sources in the solar system and galaxy since launch in 1977. Due to their sensitivity, stability, and dynamic range, the spectrometers have made a remarkable number of discoveries pertaining to the Jupiter system, the interstellar medium, astronomical, and astrophysical sources. The most surprising general aspect of these results has been the wide variety of emission processes and species which have been observed. On Jupiter's disc, the emissions detected to date are H Lyman α, H Lyman β, He (584 Å), and the H_2 Lyman and Werner bands. The atomic emissions are excited by resonance scattering of sunlight, while the H_2 bands appear to be excited by particle precipitation. On the nightside disc, only H Lyman α is present. Jupiter's auroral region is clearly delineated by intense emissions of H and H_2 bands on both dayside and nightside of the planet. Emission from He is also present in the auroral regions. At Jupiter, the atmosphere was also probed by means of solar and stellar occultation experiments. The solar occultation has revealed the distribution of H_2 and H in the upper atmosphere, while the stellar occultation has probed the structure of the upper mesosphere and lower thermosphere. Current analysis indicates an eddy diffusion coefficient $\sim 10^6$ cm^2 s^{-1} with a mesospheric temperature $\sim$ 200 K. The solar occultation analysis suggests an exospheric temperature of 1450 $\pm$ 300 K. The thermospheric lapse rate appears to be $\sim$ 1 K/km. The Lyman α observations of the disc have revealed a longitudinal asymmetry in H which may reflect longitudinal asymmetries in Jupiter's magnetosphere. Strong EUV emission from a plasma torus at the orbit of Io has been observed in transitions of sulfur and oxygen ions with a possible small contribution from potassium. The effective electron temperature of the dense regions of the plasma is estimated to be 8×10^4 K. No localized EUV emission has been detected from Io, limiting mass loading at Io to $\sim 10^{27}$ ions s^{-1}. The partitioning of ion sub-species shows deviation from pure collisional equilibrium, but preliminary analysis indicates a low diffusive loss rate. The radiative cooling rate of the torus is $\sim 3 \times 10^{12}$ W. The appearance of the entire sky in the outer solar system has been mapped in the emission lines of He (584 Å) and H Lyα (1216 Å) arising from resonant scattering of the solar lines by neutral interstellar hydrogen and helium entering the solar system. Diffuse galactic EUV emission has been measured in a number of selected directions. Stellar photospheric emissions shortward of the Lyman limit of atomic hydrogen at 912 Å have been measured. Finally, spectral images, in several emission lines, have been obtained of the Cygnus Loop supernova remnant. Sections of this article review the progress in the study of these subjects and the relationships of the EUV results to the other Voyager experiments. We include a discussion of the characteristics of the instrument and the methods of spectral analysis to verify the integrity of the reported results.

1. FOREWORD

Remote sensing and spectral analysis have been primary scientific tools in ground-based astronomy, astrophysics, and atmospheric physics throughout the history of these subjects. New discoveries have always followed soon after advances in techniques and technology. In the past several years, technological and theoretical advances in the EUV spectral range have enabled quantitative spectroscopy to provide detailed information on neutral and ionized gases of atmospheric and astrophysical interest. There are several fundamental reasons that the technological advances which have opened the EUV spectral region to investigation are so important. (1) Strong resonance transitions of the most abundant atmospheric and exospheric elements, for example hydrogen and helium, occur in the wavelength region short of 2000 Å. (2) For planets, interactions among solar radiation fields, the magnetosphere, the exosphere, and the atmosphere give rise to diagnostic EUV emission on a global scale. (3) Many of the primary astrophysical interaction processes occur in the energy equivalent temperature range 10^4 to 10^6 K, producing transitions in the EUV.

The primary goal of the Voyager UV spectrometer experiment was to define the upper atmospheres of Jupiter, Saturn, and their satellites. Although the radiation environment at Jupiter severely compromised the principal UV experiments originally planned for encounter, the primary goals have been achieved and new fields of research have been opened because of the remarkable advancements and adaptability of contemporary remote sensing techniques. Sections 3, 4, and 5 discuss the results pertaining to the prime objectives—the atmosphere of Jupiter and its satellites and the intervening medium.

Secondary goals of the Voyager UV spectrometer included observations of astronomical and astrophysical interest to be performed during cruise. Also included as a secondary goal was the observation of the sky background. Although these observations were subordinate to the main mission, they have yielded the important new results discussed in sections 6 and 7. These results are unique because the Voyager spectrometers are the only instruments capable of prolonged observations in

[1] Earth and Space Sciences Institute, University of Southern California, Tucson, Arizona 85713.
[2] University of Michigan, Ann Arbor, Michigan 48109.
[3] Naval Research Laboratory, Washington, D. C. 20375.
[4] Service D'Aeronomie du CNRS, Paris, France.
[5] Permanent address: York University, Ontario, Canada M3J1P3.

Paper number 80A1465.
0148-0227/81/080A-1465$01.00

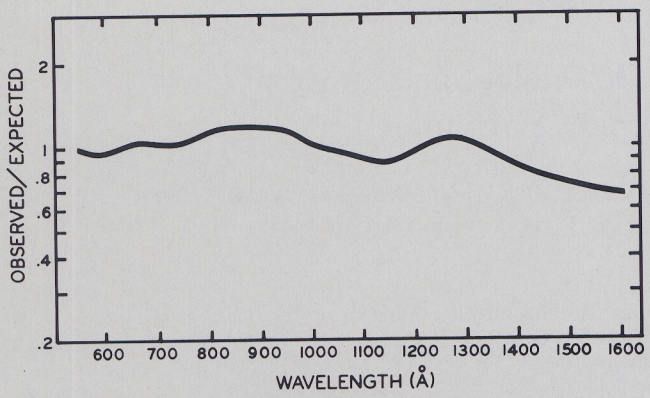

Fig. 1. The ratio of the observed solar spectrum obtained by Voyager 2 on July 25, 1978, to that expected on the basis of the calibration and the absolute solar fluxes of *Donnelly and Pope* [1973] adjusted to agree with the solar EUV emission line measurements for the day of the Voyager observations (H. Hinteregger, private communication, 1980). The important feature of this spectral ratio is its flatness (±20%) over the range 520 to 1400 Å. This flatness provides impressive confirmation of the Voyager UVS calibration. The variations which do appear are not constant and are attributed to solar intensity variation.

their wavelength range. In section 2 we describe the instrumentation and techniques of data analysis.

This report on the observations of a number of objects by the Voyager EUV instruments demonstrates the wide ranging application of the EUV spectroscopy. It also represents an important step forward in spectrography and emphasizes the continuing importance of the search and discovery nature of spectroscopic techniques.

2. INSTRUMENTATION

a. *Introduction*

A full description of the ultraviolet spectrometer is given by *Broadfoot et al.* [1977]. This instrument represents a significant departure from previously flown spectrometers in this spectral region. Therefore in this section we outline the realized inflight performance of the spectrometer and exhibit some of the novel data handling techniques made possible with such instrumentation. The instrument contains no moving parts and can best be described as an objective grating spectrograph with a one-dimensional image intensifier tube at its focal plane. The wavelength range 500 Å to 1700 Å is recorded simultaneously in 128 contiguous intervals. Low reflective efficiency constrains the instrument to a single reflection. It contains a normal incidence concave grating blazed at 800 Å in the first order. The instrument has two observational ports, separated by 20° in pointing direction. The small aperture, with a collection area of 0.78 cm^2, is used to observe the solar spectrum for the occultation experiment. The main airglow port has a collection area of 21.2 cm^2. The fields of view (FOV) are restricted by a mechanical collimator. The size of the airglow field of view is 0.87° FW in the cross dispersion direction by 0.1° FWHM in the dispersion direction giving a spectral resolution of 33 Å.

The detector is a photon counting system utilizing a 128-element linear self-scanned anode array. The array collects the output of a dual or chevron microchannel plate (MCP) electron multiplier. Photoelectrons are produced for detection by the diffracted radiation focused on the bare MCP in the 500- to 1250-Å region. In the 1250- to 1700-Å region, a MgF_2 filter coated with CuI acts as a photoelectron source for the MCP input. Further detector details are given by *Broadfoot and Sandel* [1977].

It is important to note that the design of the instrument presents a considerable advantage in providing data that facilitate accurate analysis. We emphasize the following points. (1) Each channel in the spectrum is accurately fixed in wavelength location. The lack of moving parts has allowed the establishment of accurate line shape functions and matrices for the removal of instrument artifacts, for correction of second-order spectra of short-wavelength lines, and for correction of internal instrumental scattering of the incoming radiation. (2) The entire wavelength range is detected simultaneously in a manner similar to a classical spectrograph using a photographic plate. The instrumental function is therefore not compromised by the small amount of pointing motion during the spectral integration interval. (3) The response is temporally stable as discussed below. No change (to ±10%) in the response of the Voyager 2 instrument has been detected since launch in 1977. (4) The noise background is low. The noise is produced by a combination of cosmic ray events and events from the radioisotope thermoelectric generators powering the spacecraft. This noise rate is almost constant at 2.5×10^{-2} $anode^{-1}\ s^{-1}$.

These characteristics allow accurate synthesis of observed spectra. Emissions covering a dynamic range of 10^4 are measurable given sufficient integration time. Observed emission lines, if not badly blended, can be located to within ±1Å in wavelength.

In the remainder of this section, we present a detailed examination of several aspects of the Voyager spectrometers which have an important bearing on a number of the observational results discussed here. The photometric stability of the UVS is of fundamental importance for two reasons: first, in comparing observations at Jupiter between the two encounters, and second, in our ability to relate Voyager observations to the other ultraviolet observations. The discussion of spectral analysis illustrates various observational modes of the instrument and data handling techniques.

b. *Stability*

Observational evidence has conclusively demonstrated that the long-term photometric stability of the instrument, expected on the basis of thorough and comprehensive prelaunch testing, has been realized (J. B. Holberg et al., manuscript in preparation, 1981).

The long-term stability of the instrument has been evaluated in several ways. (1) Intercomparison of a limited number of pre-Jupiter encounter stellar observations were made. (2) Observations of the same area of the Cygnus Loop [*Shemansky et al.*, 1979*b*] by Voyager 2 over a 2-year period are consistent with no change at all in the instrumental sensitivity. (3) Four stars were used for a detailed study of any possible changes in instrument response from the time period just prior to Voyager 2 encounter (July 5, 1979) to July 18, 1980.

The stability evaluation addresses the two instruments separately. Comparisons of stellar observations made between November 6, 1977, and May 1, 1980, showed that the Voyager 2 instrument sensitivity was constant to ±10% over this period, which included Jupiter encounter. On a shorter time scale, repeated observation of four stars between April 25, 1979, and July 18, 1980, allow us to conclude that the instruments have exhibited no secular trends in sensitivity to the 2% level and that variation in the stars themselves is less than 5%. The Voy-

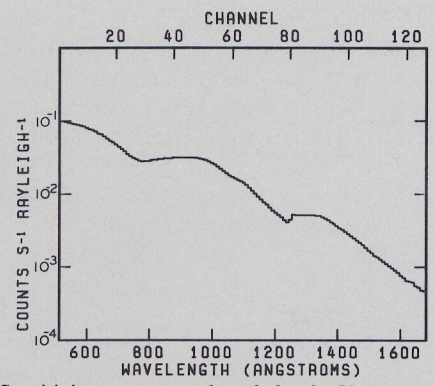

Fig. 2. Sensitivity versus wavelength for the Voyager 2 UVS. This curve applies to a monochromatic emission line whose source fills the field of view uniformly.

ager 1 instrument shows comparable stability since Jupiter encounter (March 5, 1979) using the same four stars. A drop in sensitivity of the Voyager 1 instrument was caused by the intense radiation environment near Jupiter. During the passage through the inner Jovian magnetosphere, radiation-induced counting rates reached unexpectedly high levels, and the detector gain was degraded as a result. The instrument stabilized after a few days, but the counting thresholds of the anodes of the self-scanned array had departed slightly from their pre-encounter state. The gain decrease expected on the basis of life tests [*Sandel et al.*, 1977] agrees with the measured sensitivity decrease of about 30%. This change has been documented using pre- and post-Jupiter observations of the same star and by cross comparison with Voyager 2.

c. *Calibration*

An extensive calibration was performed throughout the entire wavelength range of the spectrograph. The laboratory calibration was based on calibrated channeltron detectors. The detector calibrations are traceable to NBS standard photodiodes. The efficiencies of the gratings and detectors were

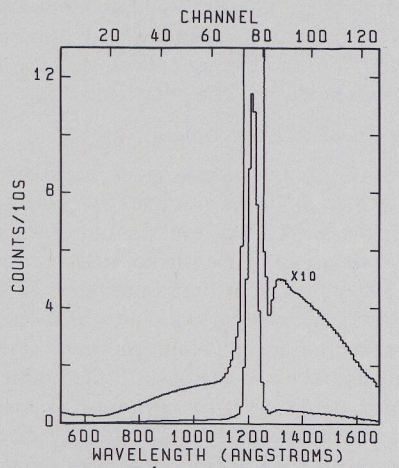

Fig. 3. Instrumental response function to a 1-kR emission line at 1216 Å. This synthesized spectrum shows the instrument's response to a monochromatic emission source filling the field of view. The width of the line (approximately 8 channels) results primarily from the 0.1° half-width of the field of view, which corresponds to 33 Å or 3.5 channels. The line is further widened by spreading of the electron cloud in its travel from the microchannel plate to the anode array. Scattering within the instrument, especially at the grating and at the edges of the apertures in the collimator, produces the wings extending over the spectrum.

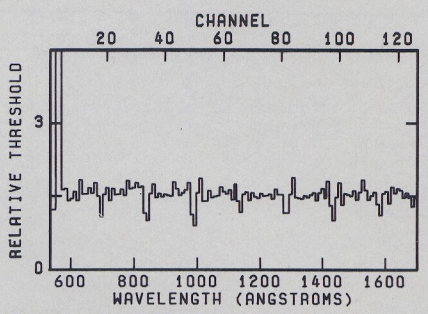

Fig. 4. Counting thresholds for each of the 128 anodes of the UVS detector. The thresholds of anodes 3 and 4, which are about 5 times higher than those of nearby anodes, are off scale. The 16-anode periodicity is a consequence of the techniques used in manufacturing the anode array.

measured separately. Then the whole instrument was calibrated, and the results were consistent with the expectations from the component efficiencies. The calibration was reproducible on retest to 5%. The transfer error from the NBS photodiode is estimated to be ±15%. We attempted to achieve high detector quantum efficiency at wavelengths longward of 1250 Å by use of a CuI photocathode. Some degradation of the photocathode sensitivity at the long wavelengths was experienced in the thermal vacuum tests which were performed at JPL. The degradation was sufficiently small that retrofitting of the instrument was not warranted. Further degradation of the photocathode (1250–1700 Å) was experienced through the launch process. In flight, stellar calibration of both instruments showed that a change in sensitivity had taken place longward of 1340 Å. The region shortward of 1250 Å, where the microchannel plate is bare, showed no degradation in many comparative studies with stellar and solar observations from rockets and satellites. This study has been described by J. B. Holberg et al. (manuscript in preparation, 1981). The ratio of a recorded solar spectrum to the solar spectrum of *Donnelly and Pope* [1973] is shown in Figure 1. The intensity of the Donnelly and Pope spectrum was adjusted to the time of the Voyager observation by use of satellite data supplied by H. Hinteregger (private communication, 1980). The ratio in Figure 1 demonstrates our ability to make photometric comparisons over the whole wavelength range of the instrument in spite of the large change in sensitivity from 500 to 1700 Å.

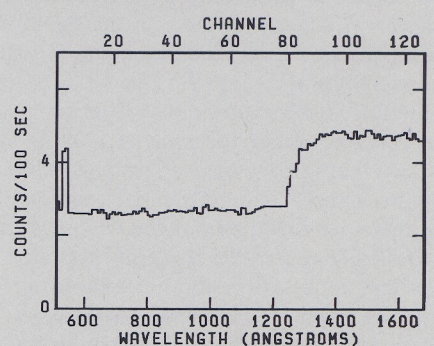

Fig. 5. A spectrum of the noise induced by gamma rays from the RTG's. An optical calibration plate served as a dark slide for this measurement. A weak signal at 1216 Å due to the reflection of the sky background has been removed from the data. The step near channel 80 corresponds to the edge of the MgF_2 filter and CuI photocathode. Evidently, this combination augments the sensitivity of the bare microchannel plate to gamma rays. The response of the detector to this noise source has remained unchanged in the 3 years since launch. The intrinsic noise rate of the detector contributes only about 10% of the total noise.

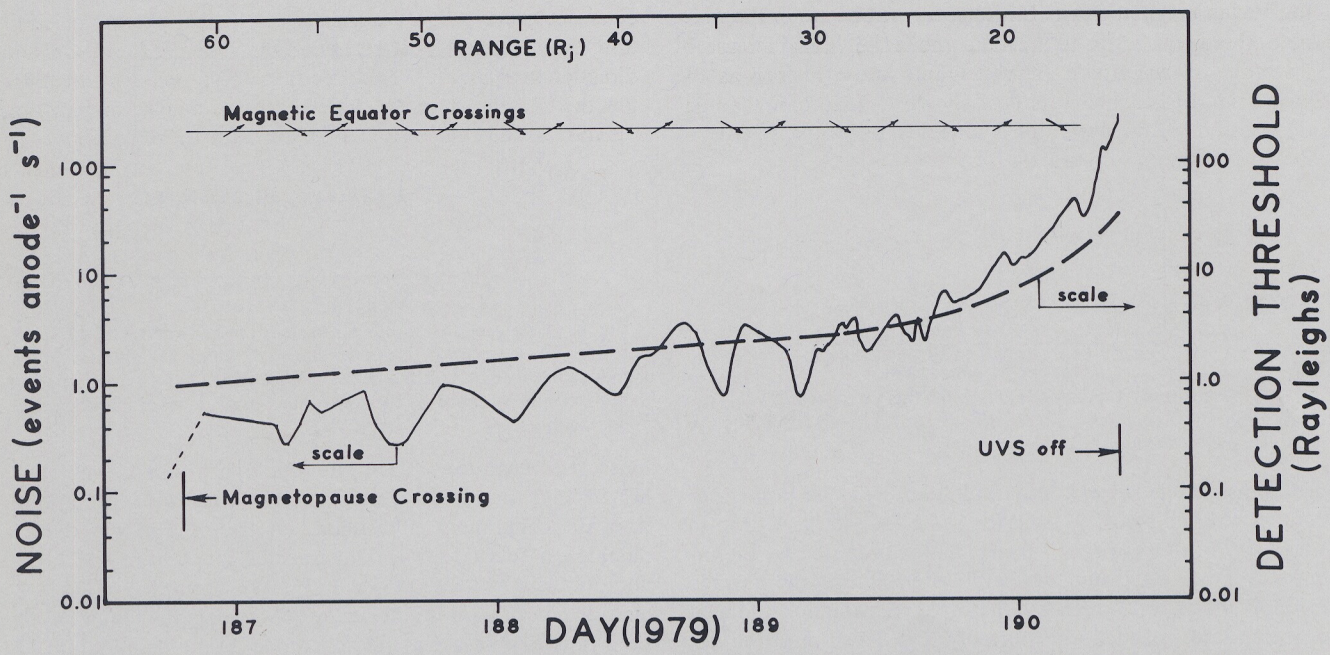

Fig. 6. Radiation-induced noise and detection threshold. Noise from the Jovian high-energy radiation field appeared at the magnetopause crossing about 60 R_J and was sensitive to the position of the magnetic equator relative to the spacecraft. The threshold of detection refers to a monochromatic line filling the field of view at 700 Å. An integration time of 1000 s was used and the assumption that the signal $S = 3(N)^{1/2}$. The curve would have to be adjusted by the sensitivity for other wavelengths.

The sensitivity curve for the Voyager 2 instrument is shown in Figure 2. The grating was chosen to favor the short wavelengths; it was blazed at 800 Å. The combination of a drop in grating efficiency toward longer wavelengths and the drop in channel plate photon efficiency is responsible for a fairly low sensitivity longward of 1100 Å. In a future instrument of this type, the sensitivity could be improved by at least an order of magnitude in this wavelength region by newer technology.

d. Instrumental Scattering

Not only was the efficiency to line emissions measured, but the instrument was illuminated long enough to evaluate internal scattering at each of 50 wavelengths throughout its spectral range. These measurements show that the typical response of a channel separated by 50 Å or more from a 'stellar' emission line at 1000 Å is less than 0.5% of the signal in the line. Figure 3 shows the scattering produced by an extended monochromatic emission line at 1216 Å. This wavelength is transmitted by the filter-photocathode, so scattering under the filter is more pronounced than for a line at 1000 Å. Taking into account the fact that signal counts are spread into about seven channels, scattering 50 Å short of the line center is about 0.7% of the total signal (summed over seven channels) in the line. Longward of the line center, the scattering is at most 1% of the signal in the line. Since the calibrations allow the prediction of a scattering spectrum for a line at wavelengths of each of the 128 anodes, we have been able to prepare a scattering matrix operator. The application of this operator to discrete emission lines produces a synthetic spectrum which matches the characteristics of the instrument exactly. Scattering in a recorded spectrum can be removed using the inverse matrix operator. This technique has been demonstrated in our published work [cf. *Shemansky et al.*, 1979*a*, *b*] and Figure 27 of this paper.

e. Fixed-Pattern Noise

We have mentioned that the detector has 128 anodes [*Broadfoot et al.*, 1977; *Broadfoot and Sandel*, 1977] in a linear array. The array, manufactured by Reticon Corporation, is a self-scanned device. When the anodes are scanned after being illuminated by a uniform or flat field of electrons, it is found that the signal varies from anode to anode. The exactly reproducible pattern of this variation is called the 'fixed-pattern noise.' Because of this pattern in the detector output, each anode-channel plate combination must be treated as an individual photomultiplier. The fixed-pattern noise can then be considered as the detector threshold. Figure 4 shows the fixed threshold pattern for the Voyager 2 spectrometer. This is similar to a flat field correction. The corrections are made to 1%.

f. Radiation-Induced Detector Noise

The detector shot noise or dark count rate measured in the laboratory was 3×10^{-3} events anode^{-1} s^{-1} [*Broadfoot et al.*, 1977], a very low level. This level has not been realized in space flight. There appear to be two sources of the noise background in flight, γ rays from the radioisotope thermoelectric generators (RTG) and cosmic rays and γ rays from the sun. An increase in the noise count rate has been correlated with solar flare activity. The correlation with the high-energy particle detectors on the spacecraft occurs only for peaks in activity, indicating the steady state level from solar cosmic rays is small compared to the continuous background from the RTG's. The background noise has been at a constant level of about 2.5×10^{-2} events anode^{-1} s^{-1} since shortly after launch. The typical radiation induced noise spectrum shown in Figure 5 was obtained by using the calibration plate as an instrument dark slide.

The detector noise stayed essentially at the cruise level of 2.5×10^{-2} events anode^{-1} s^{-1} until the spacecraft penetrated

the Jovian magnetopause. Initially, the mean rate in the magnetosphere was 2.5×10^{-1} events anode^{-1} s^{-1}, an increase of an order of magnitude. The radiation noise history as the spacecraft approached Jupiter is shown in Figure 6. Modulation caused by the motion of the magnetic equator, relative to the spacecraft, has a clear signature.

g. Threshold of Detection

The threshold of detection of an emission line changes with the type of observation being made. In deep space, when extended observing periods are available, the threshold is related to time. The signal to noise ratio

$$R = \frac{St}{(St + Nt)^{1/2}}$$

where S is the signal count rate, N is the noise count rate, and t is the integration time. An integration time of 100 hours (3.6×10^5 s) is a practical working period. For a signal to noise ratio of three, where the noise includes internal scattering (4.0×10^{-2} events anode^{-1} s^{-1}), a monochromatic emission line which fills the field of view can easily be detected. At 700 Å the detection threshold would be about 2×10^{-2} R.

As the spacecraft approaches a planetary system, observing times are comparatively short. Periods of 1000 s become practical. Here we use the same criterion for the threshold of detection as *Broadfoot et al.* [1977]. For low noise conditions, we will require 25 events to be recorded for a detectable signal. As the noise increases, the signal must be $3(N)^{1/2}$. Under these conditions the threshold of detection for low noise is 0.5 R. This level obtains until the noise rate reaches 0.75 events anode^{-1} s^{-1}, just inside of the magnetopause. A curve is drawn on Figure 6 to represent the rising threshold. We found that data inside of 30 R_J were no longer useful.

h. Spectral Manipulation

There are several corrections to be made to the raw data: these corrections must be made in the correct order to extract the EUV signature. The fixed-pattern noise correction is made first because all events recorded by the detectors are subject to the threshold level. Radiation induced noise is removed next. The radiation noise spectrum of Figure 5 is scaled to the integration time of the observed spectrum and subtracted from it. Most of the spectral comparative work is done at this stage; an example is given in Figures 26 and 27. In order to convert a spectrum to absolute flux units, the scattering inverse matrix is used to remove the scattered contribution from the strong lines; this is illustrated in Figures 27*a* and Figure 27*b*, where scattering has been removed. Finally, the sensitivity curve can be applied.

Another approach to spectral comparison is to begin with a synthetic line spectrum, then use the instrument-broadening functions and the scattering matrix to construct a synthetic comparative spectrum. An example of this process was given by *Shemansky et al.* [1979*a*, *b*]. The response of the instrument to predicted atomic line intensities is demonstrated in Figure 28, where atomic carbon lines are synthesized. It is worth noting again that unblended atomic lines can be located to within ±1 Å by this synthesis method.

i. Spectral Analysis for a Point Source

The fields of view (FOV) of the Voyager instruments are considerably larger than those of most astronomical spectrometers designed to observe individual stellar spectra. In addition, the response function across the FOV in the dispersion direction is triangular. The precision aperture stops which define the FOV produce a 0.1° (FWHM) triangular transmission function in the dispersion direction as mentioned above. In general, a stellar observation with the Voyager instruments does not consist of obtaining a single spectrum or the simple integration of many spectra but is a dynamic process involving an analysis of the spectrum as it is recorded with the star at many different positions in and out of the field of view. Because the spectrograph is not a scanning instrument and because each spectral channel is defined by a fixed anode, the response of the instrument to a stellar or diffuse source can be measured and specified to a high degree. This property permits the type of observations which we will now describe.

For an accurate measurement of its true brightness, a star must transit the central portion of the field of view, because of the triangular transmission function. Stellar observations are designed with this fact in mind. The FOV is either scanned across the star with an elevation motion of the spacecraft scan platform or allowed to drift over the star due to the slow limit cycle motion of the spacecraft's attitude control system. In either case, the 'pointing' information available from the attitude control system and scan platform position sensors permits the reconstruction of the relative position of the star with respect to the center of our field of view with a high degree of precision (0.01°, or 1/10 of our FOV width, is a common working tolerance). From this knowledge of position and the well-defined response of the instrument, it is possible to locate spectra acquired when the star was on the optical axis, correct off-axis spectra for spectral shifts and attenuation by the transmission function, and locate source-free background spectra for later subtraction.

Figure 7 shows a three-dimensional plot of an observation of β Ori with the Voyager 1 instrument: it illustrates the many considerations involved in a stellar observation and demonstrates that all of the pertinent information is available within the one data set.

Figure 7 demonstrates the use of the spacecraft limit cycle motion to obtain the required information for a weak source like β Ori (less than 1 count anode^{-1} s^{-1}). This motion causes the FOV to move in a random but continuous and smooth manner with respect to a point in space. The motion (±0.5° or ±0.16° depending on attitude control programing) is recorded with good accuracy, as mentioned above. Through our software, the motion is resolved into its components across and along the slit of the spectrometer. The position of the FOV with respect to the mean direction is recorded and accompanies each spectrum. With this information, the spectra can be taken out of their time sequence and arranged in a two-dimensional array according to position along and across the slit. The effect of this procedure is to stop the motion of the spacecraft, but more importantly, it produces a two-dimensional image in space. In all but the slowest spacecraft data rate and narrowest attitude control deadband, the integration times (3.84–576 s) are short enough to obtain spectra at spatial resolutions smaller than the FOV.

Knowledge of the source position along the slit is not very important for a point source observation, because the spectral response is known and is flat to within 4% in this direction. Motion across the slit is significant. Figure 7 shows only the one spatial dimension perpendicular to the slit. In other work,

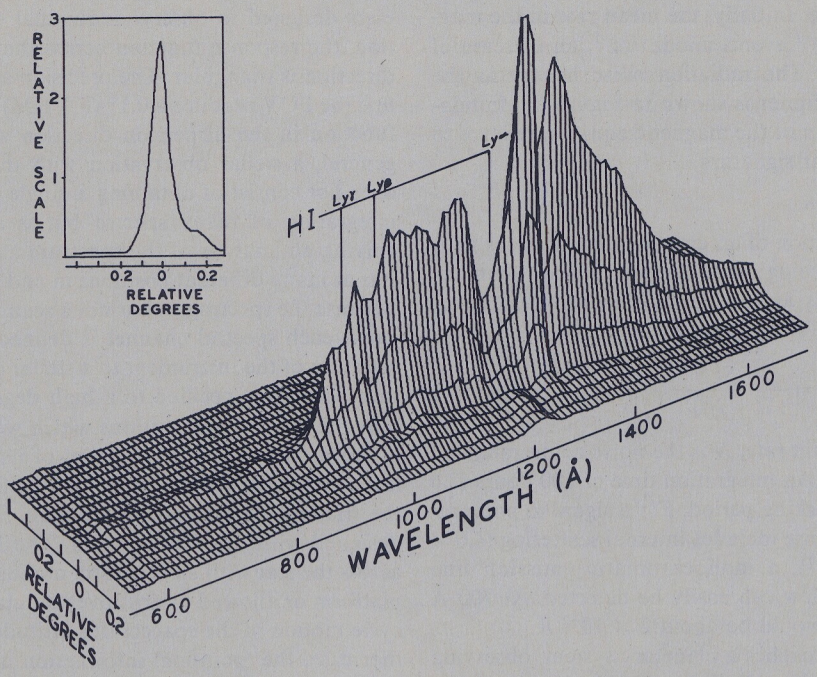

Fig. 7. The spectrum from a point source, β Ori. The limit cycle of the spacecraft, ±0.5°, causes the source to move through the FOV of the spectrograph. Because the instrument is an objective grating design, the spectrum moves in wavelength as it crosses the slit; the view was selected to show the alignment of the Lyα notch at successive positions across the slit. This is a relatively weak source in the far UV (B8Ia, $m_v = 0.8$), but it was selected because of the companion features which are apparent in these data. Scattering to wavelengths shorter than the Lyman limit when the star is in the field is evidenced by ridges in the dispersion direction. Ridges at right angles, 584-Å and 1216-Å positions, show the presence of the solar He I and H I emissions backscattered from the interplanetary gas of interstellar origin. A second star (BS 1704, B-V = −0.14, $m_v = 6.38$) 0.15° from β Ori produces a bulge in the 900- to 1200-Å region. This star is much weaker and the spectral content suggests it is hotter than β Ori. In practice, the central spectrum is used for photometry. Corrections are made by integrating the background from the same data set, which has no stellar contamination, scaling and subtracting from the central spectrum. The inset shows the transmission function of the UVS airglow port as defined by the sum of the 911- to 1170-Å signal from β Ori. The location of BS 1704 is clearly evident as a bump to right of the central peak. The spatial bins used for this figure are 0.04° in the dispersion direction.

with extended nonuniform sources, both dimensions are used.

By use of the technique described above, weak signals can easily be recognized against the background, and suitable locations of background correction spectra can be identified. In Figure 7, data located more than 0.2° off axis have no stellar contamination, and the sum of these spectra would be used as the background correction to eliminate the radiation-induced noise, as well as the interplanetary H and He emission from the stellar spectrum. For bright stars, this correction is unimportant.

The particular spectrum for which the star was in the center of the slit would be used for analysis. The shape of the instrument response function (Figure 7 inset) verifies that the spectrum is clean in spite of the weak source (BS 1704, B-V = −0.14, $m_v = 6.38$) which is located 0.15° from β Ori in the narrow slit direction. Once the appropriate background correction has been made to the stellar spectrum, instrumental scattering is removed by use of the inverse scattering matrix (see Figure 27), and the spectrum is ready for calibration. To show the relative importance of the scattering correction, we note that for a hot star whose continuum peaks in the vicinity of 1000 Å less than 2% of the 1000 Å signal is scattered into channels near 600 Å. We have studied this effect carefully because of its implications for observations of EUV sources such as HZ-43, as reported in section 6*b*.

It is difficult to define a threshold of sensitivity for stellar sources because the range of signal levels in the far ultraviolet is very sensitive to the stellar temperature. In visual magnitudes, β Ori is $m_v = 0.08$, the satellite in the spectra BS 1704 is $m_v = 6.38$, whereas our experience observing HZ 43 ($m_v = 12.86$) and other very hot stars indicates that we can obtain useful spectra for unreddened, high-temperature ($T_{\text{eff}} > 35{,}000$ K) objects of visual magnitude less than 13.

3. Atmospheric Observations

a. Introduction

Airglow emissions in a planetary atmosphere may be excited by several mechanisms: resonance scattering, photo-dissociative excitation, electron excitation, dissociative-electron excitation, chemical reactions, radiative recombination, etc. By performing a spectral analysis of the airglow features, one can obtain information on the composition and physical state of the upper atmosphere. When the airglow features are excited primarily by electron excitation, as are the H_2 bands observed on Jupiter, then we can obtain information on the intensity and energy spectrum of the particles giving rise to the excitation.

By measuring the absorption of a reference spectral source, e.g., the sun or a star, as the source passes behind the planet, we can obtain information on the average scale height of the atmosphere. By doing this at several wavelengths, it is possible to analyze the composition of the atmosphere. If the atmospheric composition is determined from this information, one may deduce a temperature for the region probed by the occultation experiment.

One of the important atmospheric parameters to be deter-

mined by the UVS experiments was the eddy diffusion coefficient K at the homopause. It turned out to be possible to do this in several independent ways. The occultation experiment implied a value of K by the onset of hydrocarbon absorption in relation to the background density determined from the same experiment. The airglow experiments also implied values of K, although in this case, the analysis is not as convincing, perhaps since there are complications due to precipitating particles. Modeling the ionosphere also leads to a value of K, although in this case, as for the dayglow data, it is not clear that the models are as yet complete.

Prior to the Voyager encounter, information on Jupiter's upper atmosphere was obtained from rocket observations of Jupiter's spectra in the 1100- to 1600-Å range. Earth-orbiting satellites have also provided useful information on Jovian airglow. The Pioneer observations of Jupiter yielded information on hydrogen and helium emissions, while the radio occultation experiment provided measurements of Jupiter's ionosphere. A review of pre-Voyager Ly α measurements [*Cochran and Barker,* 1979] seemed to indicate that Jupiter had a changeable upper atmosphere [see *Clarke et al.,* 1980]. Comparison with Voyager confirms this. As for Pioneer, there are two experiments that provide overlapping data on the same regions of the upper atmosphere, the UVS and radio occultation experiments. This permits the models developed to be compared for consistency. With the combination of pre-Voyager and Voyager measurements, it is becoming possible to piece together a temporal picture of the Jovian upper atmosphere. This picture may yield some insights into the details of upper atmosphere energetics and the interaction of the magnetosphere with the atmosphere.

In the rest of this section, we shall discuss in detail the results obtained from the emissions measured on the disc. This will be followed by a discussion of the results obtained from the occultation experiment. A general comparison of the compatability of these observations follows. Finally, we discuss the preliminary analysis of the auroral observations.

b. *Atmospheric Emissions*

The spectral features expected in the wavelength range of the UVS from an atmosphere consisting mainly of H_2, He, and H are the H_2 Lyman and Werner bands, He 584 Å, and atomic hydrogen emissions. A typical disc spectrum obtained with the UVS is shown in Figure 8. All the above emissions are present plus some lines from Io's plasma torus. In addition there are two unidentified features. One is at 926 Å; the other feature is at 1570 Å. One of the surprises in the disc spectrum (exclusive of the auroral region) was the intensity of the H_2 bands. The bands do not have the spectral structure, and are much too bright, to be attributed to resonance fluorescence of sunlight [cf. *Carlson and Judge,* 1971]. Assuming that electron excitation is the source and then calculating a synthetic spectrum, we estimate the total intensity in the Lyman and Werner bands to be 2.8 ± 1.0 kR (D. E. Shemansky et al., manuscript in preparation, 1981). This implies a total energy flux of 0.26 ergs cm^{-2} s^{-1} over the dayside disc. The energy deposition rate given here implies a factor of ~10 greater excitation efficiency than earlier published figures [*Sandel et al.,* 1979] due to an error in energy conversion in the calculation (D. E. Shemansky et al., manuscript in preparation, 1981). The average energy of the incoming electrons may be estimated from the shape of the H_2 band emission spectrum. Figure 9 shows a synthetic spectrum of the Lyman and Werner bands for electron excitation at two temperatures, 100 and 1000 K. The emission lines were convolved with the instrument function (see D. E. Shemansky et al.). It is assumed that the bands are excited by electron impact of H_2 [*Stone and Zipf,* 1972; *Srivastava and Jensen,* 1977]. The fluorescence distribution is calculated using the transition probabilities of *Allison and Dalgarno* [1970] and *Dalgarno and Stephens* [1970]. The atmosphere was assumed to be isothermal, and only transmission of the bands through the atmosphere was allowed for. For both temperatures the lines connected to $v'' = 0$ are absorbed out for base densities $\geq 10^8$ cm^{-3}, while for the 1000-K model the $v'' = 1$ connected lines are also absorbed out at larger densities. Some of this absorbed emission will reappear as fluorescence at longer wavelengths. This is not included in the calculations.

It is apparent from Figure 9 that the feature at 1106 Å is a

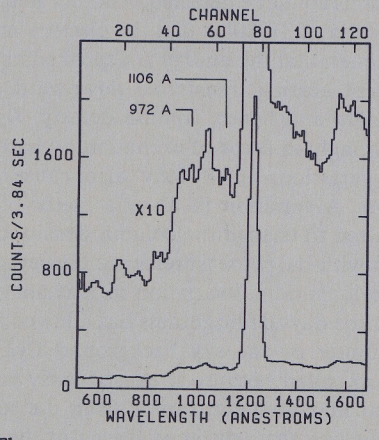

Fig. 8. The east-west map sequences consisted of scanning the planet from west to east in approximately equal latitude steps. During an individual scan the UVS stopped at 11 locations on the disc and accumulated counts. The spectrum shown in this figure is an average of the spectra observed at equatorial latitudes (free from auroral emission) which were obtained throughout one Jovian rotation. The spectrum is thus representative of equatorial regions at the subspacecraft point.

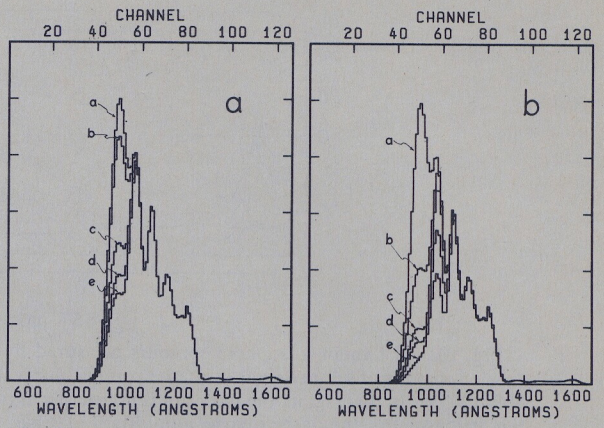

Fig. 9. Synthetic spectra of the H_2 Lyman and Werner bands as viewed by the Voyager 2 spectrometer, using the parameters discussed in the text. The excitation of the H_2 bands was assumed to occur in a layer in an isothermal atmosphere with the maximum in the excitation peak about 1/4 of a scale height above the base of the atmosphere. The curves show the transmissions for the various model atmospheres. (*a*) $T = 100$ K: Curve *a* is for an optical depth of zero. Curves *b*, *c*, *d*, and *e* are for isothermal atmospheres with base densities of 10^7, 10^8, 10^9, 10^{10} cm^{-3}, respectively. (*b*) $T = 1000$ K: Curve *a* is for an optical depth of zero. Curves *b*, *c*, *d*, *e* are for isothermal atmospheres with base densities of 10^8, 10^9, 10^{10}, 10^{11} cm^{-3}, respectively.

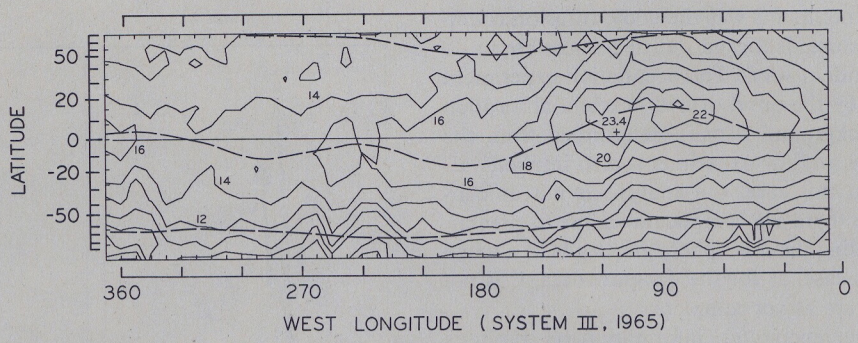

Fig. 10. H Lyman α isophote contours measured by Voyager 1 during the north-south map sequence. Contours are labeled in units of kilorayleighs (kR); the contour interval is 2 kR. The H Lyman α intensity bulge is clearly apparent near 80°–120°W. In this region, the intensity is noticeably asymmetric about the spin equator. It is much more symmetric about the drift equator, the dashed curve at mid-latitudes [see *Dessler et al.*, 1981]. The dashed curves near the poles show the track of the foot of Io's flux tube.

good monitor of the total excitation independent of the depth at which the electrons deposit their energy. The ratio of the other features to this feature provides a measure of the depth of the excitation source. From the relative intensities of the features at 972 and 1106 Å, it appears that the H_2 bands are excited in the exosphere, i.e., where $[H_2] \sim 10^8$ cm^{-3}. If this is indeed correct, then the flux and the altitude of its deposition are adequate to explain the hot exosphere [see *Hunten and Dessler,* 1977]. There still remains a problem, however, as to the source of these electrons. Whatever the source of the electrons, it must have a diurnal trigger, since the H_2 bands are not (<300 R) observed on the nightside.

These electrons may also be a source of other emissions. For example, Lyα may also be excited by dissociative excitation of H_2. However, only about 300 R is expected on the basis of the H_2 band intensity. Electron excitation of atomic H is also a possibility.

At the time of Pioneer encounter with Jupiter the measured Lyα brightness was 400 R [*Carlson and Judge,* 1976]. By the time of Voyager encounter the Lyα emission on the disc had a brightness of 15–20 kR at the subsolar point. Apart from the increase in intensity, another surprising feature was the spatial structure in Lyα. *Sandel et al.* [1980] deduced that at the time of the encounters there was a persistent longitudinal asymmetry in the Lyα intensity. Analysis of the data presented by *Sandel et al.* [1980] has been extended to reveal the north-south structure in the Lyα brightness as shown in Figure 10. The pronounced north-south asymmetry near 110°N may be due to coupling with the magnetosphere [*Dessler et al.*, 1981]. The longitudinal asymmetry also appeared in the measurements of Lyα on the nightside. The intensity on the nightside varied from 700 to 1000 R [*McConnell et al.*, 1980].

Pre-Voyager models of Lyα emission on the Jovian disc in nonauroral regions attributed the emission to scattering of the solar Lyα line with a minor contribution from dissociative excitation of H_2 [*Carlson and Judge,* 1971; *Wallace and Hunten,* 1973]. The source of H in the upper atmosphere is ionization of H_2 by solar EUV photons. The subsequent ion-molecule reactions result in net dissociation of H_2. The column amount of H above the CH_4 layer depends inversely on the time constant for flow to the lower atmosphere. This in turn depends on the eddy diffusion coefficient K. Higher values of K yield lower column amounts of H and so lower Lyα brightness [*Hunten,* 1969; *Wallace and Hunten,* 1973].

At the time of Pioneer encounter the value of K deduced from the Lyα measurement was $(3 \pm 1) \times 10^8$ cm^2 s^{-1} [*Carlson and Judge,* 1974]. By the time of Voyager encounter the solar Lyα flux had only changed by a factor of 2 to 3 as compared to the factor of 40 change in the Jovian Lyα brightness. Calculations [*Yung and Strobel,* 1980; J. C. McConnell et al., manuscript in preparation, 1981] suggest that $K \sim 10^6$ cm^{2}s^{-1} at the time of Voyager encounter. These refer to the nonbulge side of the planet. Thus there have been dramatic changes in upper atmosphere dynamics since the time of Pioneer encounter. One must remember, however, that the modeling may not be complete, since sources of Lyα from e + H are not included.

The Lyα intensity bulge is a puzzle. Is it due to enhanced column amounts of H or is it due to precipitation of particles causing excitation of Lyα by e + H? *Sandel et al.* [1980] suggest that the excess intensity reflects increases in column amounts of H. The source of excess H was attributed to precipitating particles. The column increase of H required to account for the increased intensity is about a factor of 3 (J. C. McConnell et al., manuscript in preparation, 1981). *Sandel et al.* [1980] suggested that the precipitation pattern was nonsymmetric, reflecting the inhomogeneities in the magnetic field and magnetospheric plasma densities. Since there was no similar intensity asymmetry in the H_2 bands, they suggested the possibility that the energy spectrum of the precipitating particles was sufficiently hard that the energy was deposited below the homopause. In this way, H_2 would be dissociated while no emissions could be detected. Another possibility suggested by *Sandel et al.* [1980] is that the electron energy spectrum is soft enough that the energy is deposited above the H_2 and the resultant heating transferred downward to increase the H scale height and hence, column density. *Dessler et al.* [1981] argue strongly in favor of excitation by hard electrons. Longitudinal variations in K may also cause brightness changes in Lyα. A variation in K by a factor of about 4.5 would be required to change the column density of H to obtain agreement with bulge measurements. However, a mechanism to drive a longitudinal variation in K is not obvious.

No model of the dayside brightness has allowed for the illumination of Jupiter by the sky background Lyα. (The sky 'background,' so called because it caused early confusion in Lyα geocoronal measurements, arises from the scattering of the solar Lyα line by the neutral hydrogen of the interstellar wind (ISW). The ISW is just the local interstellar medium moving relative to the solar system. One person's noise is another person's signal!) However, *McConnell et al.* [1980] show that 1.4 kR of emission at the subsolar point, for an H column of 10^{17} cm^2, would be attributable to scattering of the sky background.

With the column amount of H present on Jupiter the Lyβ

emission line should be observable with the UV spectrometer. Unfortunately, it is blended with an H_2 band feature in the region of 1026 Å as shown in Figure 8. The intensity of the whole feature at 1026 Å is about 100 R. J. C. McConnell et al. (manuscript in preparation, 1981) have calculated the amount of Lyβ emission expected from scattering of the solar Lyβ line. The calculation is less straightforward than that for Lyα, since the upper $3p$ state of H may radiate a Hα photon. J. C. McConnell et al. have treated the problem by adopting the method of *Carlson and Judge* [1971] whereby scattering in the core of the line is treated according to the complete frequency redistribution (CFR) approximation and scattering in the wings according to the coherent scattering (CS) approximation. Mixing CFR and CS according to Carlson and Judge and using column amounts of H that are consistent with bulge and nonbulge intensities, J. C. McConnell et al. obtain 50 and 40 R, respectively, of Lyβ. Thus the H bulge will be much less apparent in the Lyβ data. From the calculations, it appears that not all of the observed feature at 1026 Å can be due to scattering of the solar Lyβ line. The excess of the emission at 1026 Å is probably due to H_2 band emission, with a possible contribution from e + H. The nature of the Lyβ emission may be an important boundary condition as our model of the upper atmosphere develops.

Both the Voyager 1 and 2 spectrometers have observed Jovian He 584 Å emission with an intensity of about 4 R, approximately the same intensity as Pioneer 10. The exciting solar flux, however, has increased by a factor of 3 to 6 in the interim. Figure 11 shows the disc intensity obtained from the E-W maps for V1 and V2. Also shown are two model fits to the data. *McConnell et al.* [1981] have discussed the implications of the He 584 Å observations. The intensity is sensitive to K, the temperature of the scattering region T, and the He/H_2 mixing ratio f [*Carlson and Judge*, 1974, 1976; J. C. McConnell et al., manuscript in preparation, 1981]. Analysis of the Pioneer and Voyager infrared data [*Orton and Ingersoll*, 1976; *Hanel et al.*, 1979] yields a more accurate He/H_2 ratio in the lower atmosphere than can be obtained with the UV data. *McConnell et al.* [1981] used a value for f from the IR data in their analysis in order to reduce the number of uncertainties. They deduced a value for K dependent on the temperature of the scattering region at the time of the Voyager encounters. If $T \sim 150$ K, then $K \sim 7$ to 15×10^5 cm^2 s^{-1}, while for $T \sim 1000$ K, then $K \sim 110$ to 220×10^5 cm^2 s^{-1}.

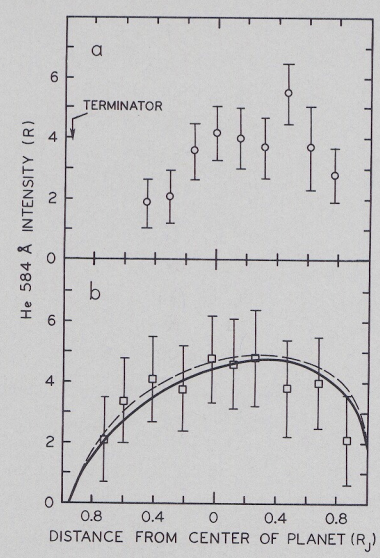

Fig. 11. The intensity of the He 584 Å emission across the planet. The four E-W scans nearest the equator from three maps have been summed. The horizontal axis is the location of the center of the slit for the center scan projected onto the Jovian disc. (*a*) The intensities for Voyager 1. (*b*) The points give the intensities for Voyager 2. The solid curve is for a model atmosphere with $T = 150$ K and $K = 1.5 \times 10^6$ cm^2 s^{-1}. The dashed curve is for $T = 500$ K and $K = 8 \times 10^6$ cm^2 s^{-1}. A phase angle of 20° was assumed for plotting the points. The models were not averaged over the slit [*McConnell et al.*, 1981].

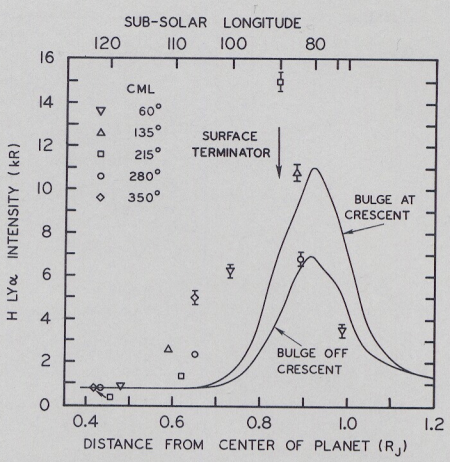

Fig. 12. Apparent intensities measured from the eastern night side and illuminated crescent portion of the Jovian disc. The five separate scans shown here were taken within 8° of the equator, but at different central meridian longitudes, (CML). For the scans at CML 60°, 280°, and 350° the Lyα bulge region was not on the crescent, but for the scans at CML 135° and 215° the bulge overlapped the crescent. The error bars show the ± 1 σ statistical error. When no error bar is shown, the size of the plotted symbol is comparable to the uncertainty. The solid curves show the apparent intensity calculated by averaging over the slit for the Lyα bulge present and not present on the crescent. The nightside was assumed to have a uniform intensity of 800 R, while the sky background had a uniform intensity of 1400 R [*McConnell et al.*, 1980].

The helium observations also suggest the presence of a helium intensity bulge out of phase with the Lyα bulge [*McConnell et al.*, 1981]. This result may be in agreement with the idea that the Lyα bulge is due to an increased column of H, since the extra H will absorb out some of the He 584 Å line. However, a longitudinal variation in K or T would also yield a similar behavior.

Lyα is the only emission detected on the nightside so far. The nightside H_2 band system intensity was less than 0.1 that of the dayside. The measurements have been discussed by *McConnell et al.* [1980]. The intensity of Lyα is between 700 and 1000 R and appears to vary with longitude. The nature and amplitude of the variation match the dayside Lyα bulge. The intensities measured across the disc are fairly uniform. The Lyα sky background illuminates the nightside of the planet. Calculations of the contribution of the sky background to the observed intensity indicate that only ~ 350 R on the nonbulge side is due to this source. *McConnell et al.* [1980] assumed that the remaining intensity was due to the excitation of H by precipitating electrons. Based on the lack of H_2 emissions and the behavior of the emission across the disc, they estimated that the electrons were soft in energy and deposited ~0.04 erg cm^{-2} s^{-1}. If this is so, then the particle precipitation pattern must be asymmetric in order to produce the observed Lyα intensity bulge.

During the observing sequence, the bright crescent was also observed. Averaging the dayside model intensities and sky background over the slit gave reasonable agreement with the observations as shown in Figure 12. Just behind the termi-

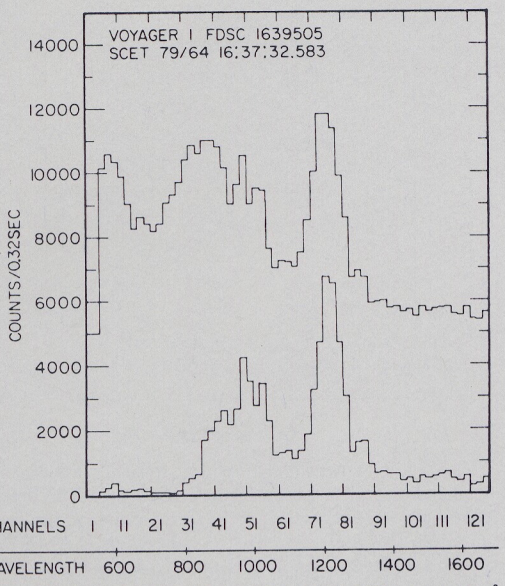

Fig. 13. Unattenuated solar spectrum in the 500- to 1700-Å range as viewed by the Voyager 1 UV spectrometer (upper curve) and after absorption by the Jovian atmosphere has begun (lower curve). The zero for the upper spectrum is offset by 5000 counts [*Atreya et al.*, 1979*a*].

nator (and at one point on the terminator), Lyα appears to be anomalously bright. As shown in Figure 12, the measured brightness is 1 to 5 kR higher than the calculated brightness expected in the region 0.6–0.8 R_J. Currently, there is no explanation for this observed behavior. There is a possibility that it is a radiative transfer effect involving multiple scattering of photons across the terminator. The aspect ratio of the atmosphere would tend to preclude this. However, the large optical depths in Lyα (10^4) make it seem more reasonable. The brightening could also be due to precipitation. The point at 0.8 R_J with an intensity of 15 kR is not due to radiative transfer effects. It suggests a precipitation source.

The nightside emission emphasizes two features of the particle precipitation pattern (1) There is a large day/night variation as evidenced in the H_2 band emission. (2) The asymmetric precipitation pattern suggested by the dayside Lyα bulge emissions of *Sandel et al.* [1980] and *Dessler et al.* [1981] is present on the nightside. However, the energy spectrum of the precipitating particles may be different on dayside and nightside.

To date, there are no indications of the source of the emission features at 926 and 1570 Å. As discussed by *Sandel et al.* [1979], the source of the latter emission is probably not H_2 Lyman bands. The feature at 926 Å is also probably not due to H_2 band emission unless it is from highly vibrationally excited H_2. Even this seems unlikely, as we would expect the signature to occur in other regions as well. Part of the 1570 Å feature may be simply solar flux Rayleigh scattered from the atmosphere. However, a feature in this wavelength region has appeared off the disc as the magnetosphere was being mapped.

c. *Occultation Experiments*

An important physical property of a planetary atmosphere is its temperature structure. Jupiter radiates 1.67 times as much energy as it receives from the sun [*Hanel et al.*, this issue]. As we go up in altitude, we find that temperature information is available in the lower mesosphere region (at a pressure level of about 1–10 dyn cm^{-2}) from visible stellar occultation measurements [cf. *Hunten and Veverka*, 1976]. Continuing up in altitude, we find that nothing more of Jupiter's temperature structure is known until we get to the exosphere. Radio occultation measurements at Pioneer encounter imply plasma temperatures ~850 K [*Fjeldbo et al.*, 1976; *Hunten*, 1976]. Since theoretical considerations [*Henry and McElroy*, 1969; *Nagy et al.*, 1976] indicate little or no disequilibrium between the electron, ion, and neutral temperatures, the neutral temperature in the exosphere at the time of Pioneer encounter was probably ~850 K. The Voyager RSS experiments [*Eshleman et al.*, 1979] indicated a similarly hot plasma temperature at time of encounter.

One of the aims of the UVS occultation experiments was to fill part of the glaring gap in our knowledge of the temperature structure in the region between the mesosphere and exosphere. The EUV observations using α Leo as a source have now provided information on the structure above 250 km as discussed below.

The first measurement of the upper atmospheric 'neutral' temperature was made by a solar occultation exercise [*Broadfoot et al.*, 1979] on Voyager 1 when UVS was used in an absorption mode. The absorption of the solar flux in the interval 500–1700 Å was studied at a range of 7 R_J as the spacecraft swung behind the planet about 4.5 hours after the Jupiter encounter. The line of sight to the sun traversed the Jovian atmosphere at continuously diminishing tangent ray altitudes. The spectra were taken every 0.32 s with a spectral resolution of approximately 10 Å as the tangent ray height changed by 19 km s^{-1}. The top curve in Figure 13 shows an unattenuated spectrum of the sun before absorption in the Jovian atmosphere commences, while the bottom curve shows substantial continuum absorption due to H_2 a short time later when the tangent ray had descended into the atmosphere. The most useful information retrieved from the experiment is the exospheric temperature. The temperature was deduced from a measurement of the H_2 scale height obtained by examining the absorption of solar flux in the range 600–730 Å (Figure

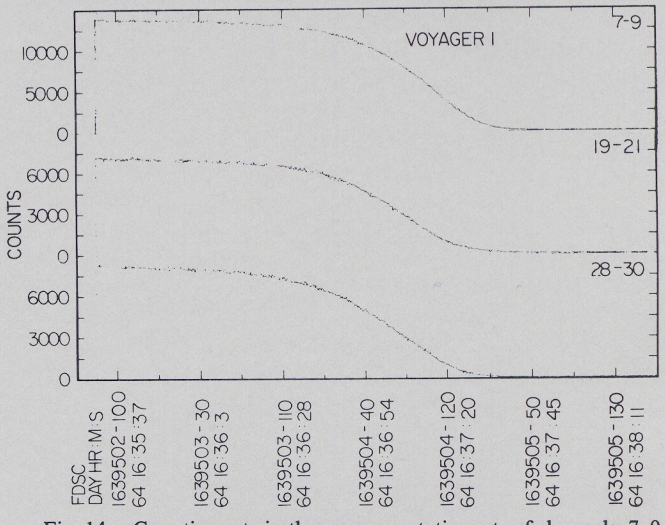

Fig. 14. Counting rate in three representative sets of channels: 7–9 (590–618 Å), 19–21 (665–692 Å), and 28–30 (702–729 Å) as a function of time during the solar occultation [*Atreya et al.*, 1979*a*]. The absorption by H_2 occurred in the height range where the H_2 density is on the order of 10^7 to 10^8 cm^{-3}. No reliable height reference was available from the solar occultation experiment. However, one can relate this H_2 density to a height of about 1500 to 2000 km above the ammonia cloud tops by using the H_2 density profile from a stellar occultation experiment (see Figure 18).

14), where the H_2 absorption spectrum is relatively flat. The neutral temperature is deduced to be 1450 ± 250 K nearly 1500 km above the ammonia cloud tops [*Atreya et al.*, 1979*a*]. The upper atmospheric neutral temperature is found to be virtually the same as the plasma temperature at essentially the same time and latitude [*Eshleman et al.*, 1979; *Atreya et al.*, 1979*a*].

The occultation data are being further analyzed and should yield information on the H to H_2 ratio in the thermosphere and on the altitude of the H_2 absorption, mentioned earlier, above the homopause. Preliminary results suggest qualitative agreement with the Lyα disc brightness data when it is borne in mind that the Voyager 1 solar entrance occultation occurred in the region of the Lyα bulge.

The experimental design at Jupiter was not optimal due to the orbit characteristics dictated by the harsh radiation environment. The problems in the data reduction arise from possible nonuniform distribution of ultraviolet intensity on the solar disc. At the time of the above observations, no spatially resolved solar flux observations were being carried out. The finite angular diameter of the sun, 0.1° at the distance of Jupiter, also obscures the height profiles of the absorbers in the deeper atmosphere. It should also be pointed out that the exit solar occultation on Voyager 1 was unsuccessful due to pointing errors and stabilization problems, and the Voyager 2 solar occultation occurred at a range of about 25 R_J, resulting in unacceptably large uncertainties in the results.

Further information on the upper atmospheric temperature was obtained from studying the occultation of the star Regulus (α Leonis, HD 87901, B7V, $m_v = +1.35$) with the Voyager 2 UVS. The tangent ray height changed by about 10 km s^{-1} during this experiment, and absorption data provided composition and temperature profiles in the deep atmosphere. Figure 15 shows a spectrum of α Leo just prior to occultation and another taken when absorption by hydrocarbons and H_2 in the Jovian atmosphere had begun. The scale height of H_2, determined from the absorption in the Lyman band system (912–1108 Å), gives the temperature profile above 250 km, while the temperature at 250 km is obtained from absorption data for hydrocarbons and H_2 Lyman bands (see later). The temperature at 250 km, determined to be 200 ± 25 K in the present analysis of the UVS observations, is in good agreement with the estimate at 150 km by the IRIS experiment

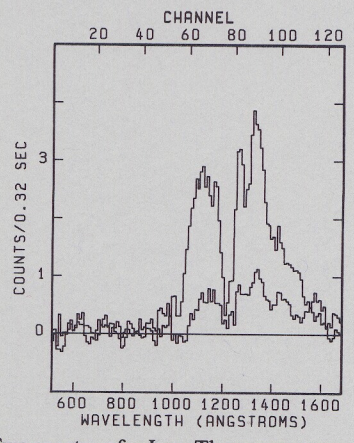

Fig. 15. Two spectra of α Leo. The upper curve shows the unattenuated stellar flux before atmospheric absorption began. The lower spectrum was taken a short time later and shows absorption in channels 45 to 120 due to H_2 Lyman and Werner bands and hydrocarbons. The peak flux from the star is 400 photons cm^{-2} s^{-1} $Å^{-1}$ at 1505 Å.

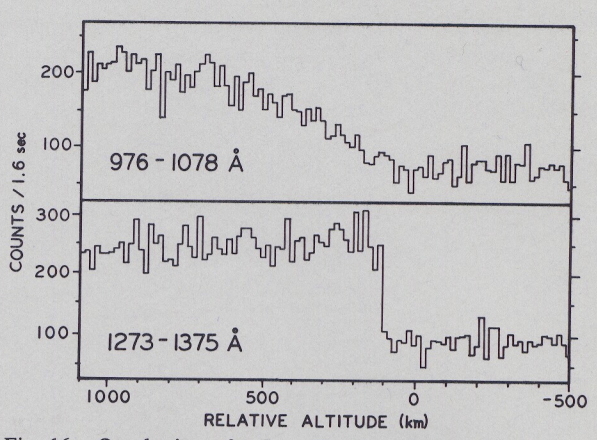

Fig. 16. Occultation of α Leo (Regulus) by Jupiter. The stellar light recorded in two wavelength intervals is represented as a function of relative altitude. Gradual absorption at 976 to 1078 Å is attributed to H_2, whereas the abrupt onset of absorption at 1273 to 1375 Å is attributed to hydrocarbons. The residual signal after the hydrocarbon occultation is a combination of high-energy particle background and Jupiter's dayglow [*Sandel et al.*, 1979].

[*Hanel et al.*, 1979]. The details of the analysis are presented elsewhere [*Festou et al.*, 1981].

As mentioned earlier, knowledge of K at the homopause level is of fundamental importance in determining the first-order vertical dynamical conditions in the upper atmosphere. We have already discussed means of obtaining K using Lyα and He 584 Å emissions. The direct detection of the homopause level is possible if absorption by methane or another hydrocarbon is monitored as a function of altitude. If the density is known at another altitude and the intervening temper-

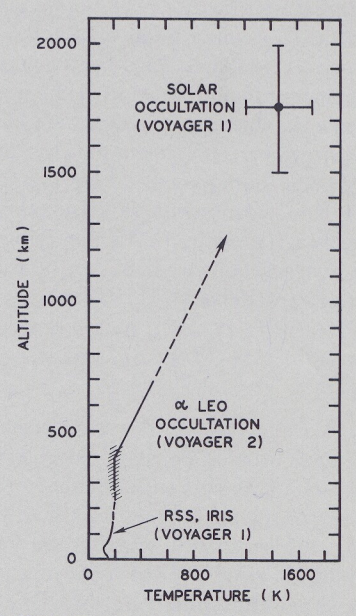

Fig. 17. Preliminary atmospheric temperature versus altitude relative to ammonia cloud [*Festou et al.*, 1981; *Atreya et al.*,1981]. The temperature profile up to 150 km is measured by the radio science and IRIS investigations on Voyager. The hatched region represents the results of temperature retrieval obtained from visible stellar occultation (see the review by *Hunten and Veverka* [1976]). The temperature retrieved from the UVS stellar occultation data is good up to 700 km and must follow approximately the dashed curve beyond 700 km to meet the UVS solar occultation data between 1500 and 2000 km and to produce the transmission at 700 and 400 km observed in the α Leo occultation. For further analysis and final results, consult *Festou et al.* [1981] and *Atreya et al.* [1981].

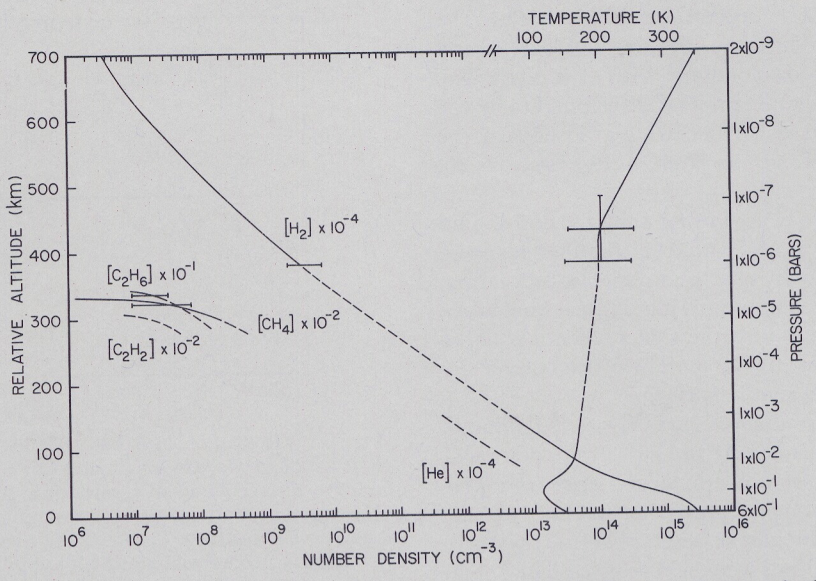

Fig. 18. Preliminary height profiles of H_2, CH_4, C_2H_6, and C_2H_2 deduced from the α Leo occultation data [*Atreya et al.*, 1981; *Festou et al.*, 1981]. The He density is simply a representation of the IRIS homospheric volume mixing ratio of 0.1 for He. The volume mixing ratios of CH_4 and C_2H_6 at 325 km are 2.5×10^{-5} and 2.5×10^{-6}, respectively, while $C_2H_2 \leq 5 \times 10^{-6}$ at 300 km. The temperature profile shown in this figure is the same as in the previous figure. Pressures on the right ordinate correspond to the altitudes on the left ordinate.

ature structure is known, then the location of the homopause also fixes the value of the eddy diffusion coefficient, since at this level the eddy diffusion coefficient must be equal to the molecular diffusion coefficient. The α Leo stellar occultation mentioned earlier measures atmospheric absorption in the range 900–1600 Å as the tangent ray height descends in the atmosphere. The absorption in the $\lambda > 1100$ Å range is caused primarily by hydrocarbons, particularly methane, ethane, and acetylene, while the H_2 Lyman band absorption occurs primarily in the range 912–1108 Å. This behavior is evident in Figure 16, where the gradual absorption in the upper panel is due to high-altitude H_2 where scale heights are large, and the sudden onset of absorption in the lower panel is due to hydrocarbons just below the homopause, where the temperatures are relatively low. The hydrocarbon data are analyzed in conjunction with the analysis of the H_2 Lyman band absorption data so that the hydrocarbon densities can be related to the background atmospheric density. This analysis, presented in detail elsewhere [*Atreya et al.*, 1981; *Festou et al.*, 1981], gives $K = 0.7$ to 2.2×10^6 cm^2 s^{-1} at the homopause.

d. Discussion

Temperature. An analysis of the radio science electron density profiles and occultation data suggests reasonable agreement for exospheric temperatures deduced from the two techniques. A comparison of Pioneer and Voyager observations suggests that the exospheric temperature has increased from 850 K to 1400 K. A number of mechanisms have been suggested for the upper atmospheric heating. One such source is vertically propagating inertia gravity waves which deposit their energy in the thermosphere [*French and Geirasch*, 1974]. Another possible source is the penetration of low-energy magnetospheric electrons [*Hunten and Dessler*, 1977]. The former source has some credence, since the existence of inertia gravity waves has been inferred from oscillations in the stratospheric and mesospheric temperatures retrieved from the observation of the occultation of β-Sco [*Elliott et al.*, 1974] and was later confirmed by the Voyager imaging data [*Hunt and Muller*, 1979]. *Atreya and Donahue* [1976] and *Atreya et al.* [1979*a*] find by solving the heat conduction equation that one can easily arrive at a temperature of 1000–1500 K for the upper atmosphere if the waves dissipate five to ten scale heights

TABLE 1. Estimates of Eddy Diffusion Coefficients K at the Homopause From Different Models

Model	Range of K, 10^6 cm^2 s^{-1}
Ionosphere	0.1–0.3
Lyα disc brightness	1–10
He 584 Å	0.7–1.5 (150 K)
	11–22 (1000 K)
Stellar occultation	0.7–2.2

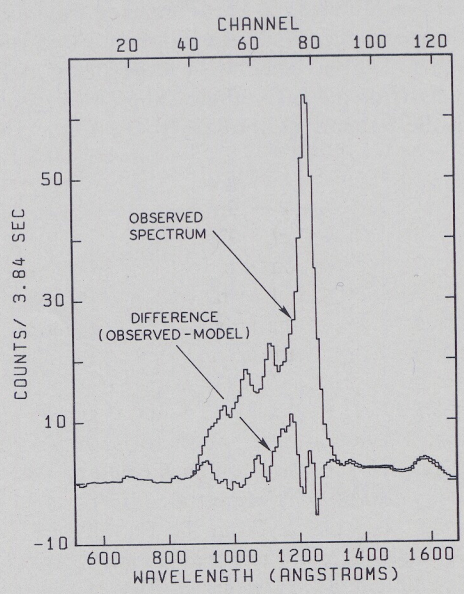

Fig. 19. A preliminary comparison of a model spectrum and an observed auroral spectrum. For the lower curve, the components of the model, H_2 bands and H Lyα line emission as well as an emission line near 1250 Å, were subtracted from the observed spectrum. The source and significance of the 1250-Å feature are uncertain.

above the homopause and deposit their energy flux, which is estimated to be ~3 erg cm^{-2} s^{-1} [*French and Geirasch,* 1974]. However, currently the level at which the waves break up is not known. From the observed temperature gradient of about 1°K/km of the thermosphere, it is also evident that inertia gravity waves may not be the primary heating mechanism, since this source would imply a much steeper temperature gradient above the homopause [*Atreya et al.,* 1981].

As suggested above when discussing the H_2 band emission, about 0.3 erg cm^{-2} is deposited in the upper atmosphere if electrons are the source of the H_2 emission. This is just what *Hunten and Dessler* [1977] require to maintain the exospheric temperature. The source of the electrons and their energization mechanism remain a puzzle. The original excitation mechanism suggested does not seem adequate [*Hunten and Dessler,* 1977].

An additional possible heat source is drag caused by a differential wind between ions and neutrals, i.e., the Joule heating mechanism. This works best in the ionospheric layers observed in the Pioneer data and suspected in the Voyager data. However, there were no measurements of winds in the upper atmosphere, so the viability of the heating mechanism must remain speculative. However, the magnitude of the differential winds needed is reasonable, 100–200 m s^{-1} at the 10^{14} to 10^{12} cm^{-3} density level.

Figure 17 shows estimates of the temperature structure above the tropopause. An important contribution to our knowledge of temperature structure has come from the measurement of the temperature in the lower thermosphere, as this further serves to constrain models of the upper atmosphere.

Eddy diffusion coefficients. The Voyager observations have led to estimates of K at the homopause from several sources including the ionospheric data, the Lyα data, the He 584 Å airglow, and the hydrocarbon absorption. The deduced values are summarized in Table 1.

Atreya et al. [1979*b*] have analyzed the equatorial electron density profiles [*Eshleman et al.,* 1979] in terms of K. They find K at the homopause level to be between 1 and 3×10^5 cm^2 s^{-1}. However, this conclusion was reached before the Lyα intensity bulge was discovered [*Sandel et al.,* 1980]. This bulge suggests that additional ionization at low altitudes due to particle precipitation may be important [*Sandel et al.,* 1980]. Since this was not considered by *Atreya et al.* [1979*b*], it may affect the conclusions regarding K deduced from their model. It is possible that the day/night behavior of the ionosphere observed by *Eshleman et al.* [1979] may be due to the particle precipitation being asymmetric [cf. *McConnell et al.,* 1980]. We note that the Voyager 1 entrance and Voyager 2 exit RSS occultations occurred in the bulge region, as did the Voyager 1 solar and stellar occultations discussed here.

The Lyα intensities observed suggest that $K \simeq 10^6$ cm^2 s^{-1} [*Yung and Strobel,* 1980; J. C. McConnell et al., manuscript in preparation, 1981]. However, if there is an additional H source, or if e + H is important, then K could be ~10^7 cm^2 s^{-1}. The He 584 Å observations suggest $K \sim 10^6$ cm^2 s^{-1} if the line scattering occurs at 150 K. From the T profile in Figure 17, 200–300 K might be more reasonable, which would suggest the $K \sim 2 \times 10^6$ cm^2 s^{-1}. However, a value of $K \sim 10^7$ with a 1000-K scattering region cannot be ruled out. An important uncertainty relating directly to the value of K should be kept in mind; measurements of solar flux at the time of encounter by H. Hinteregger (private communication, 1980) and by

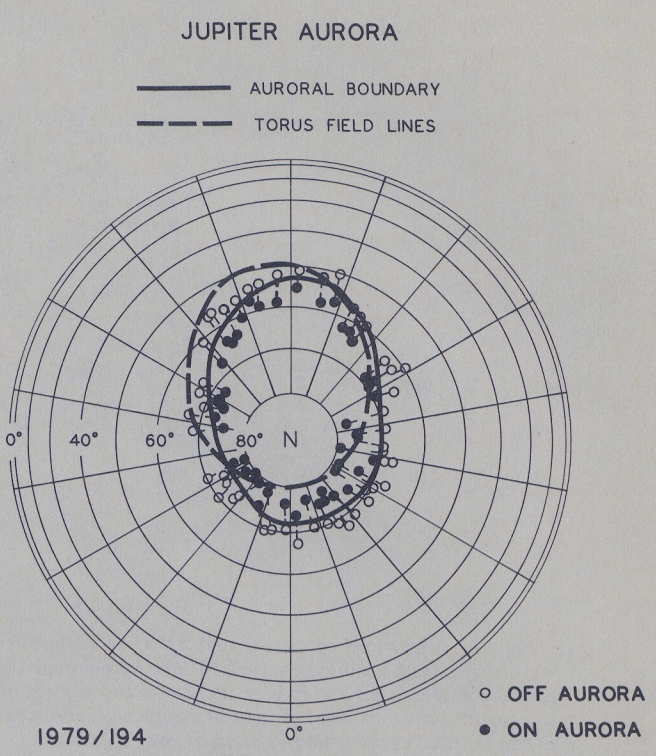

Fig. 20. In this north polar view, the slit is aligned with the (radial) lines of constant longitude. The position of the northern end of the slit when auroral emissions were and were not detected are shown by solid and open circles, respectively. The solid line shows the equatorward boundary of the auroral zones inferred from this analysis. The dashed curve shows the magnetic mapping of the orbit of Io onto the atmosphere (N. F. Ness, private communication, 1979).

Mount et al. [1980] differ by a factor of 1.6, introducing a large uncertainty in the modeling of the albedo processes.

Analysis of absorption by hydrocarbons, particularly CH_4 and C_2H_6 in the stellar occultation data, suggests $K = 1.4^{+0.8}_{-0.7} \times 10^6$ cm^2 s^{-1}. Taken together the weight of evidence, if not its accuracy, would suggest that $K \sim 10^6$ cm^{-2} s^1. In addition, the He 584 Å data imply that the atmosphere must be quasi-isothermal for several scale heights above the homopause [*McConnell et al.,* 1981]. This would tend to be in agreement with the stellar occultation data, if $K \sim 10^6$ cm^2 s^{-1}. Thus particle precipitation in the bulge region would supply the additional column of H as suggested by *Sandel et al.* [1980], and this in turn would produce the He 584 Å 'anti' bulge.

Composition. Most of the details of the upper atmospheric composition profiles were obtained from the solar and stellar occultation experiments. However, the disc emissions provide estimates of column amounts of H. Although the IRIS observations [*Hanel et al.,* this issue] give the bulk composition for $p > 10$ mbar in the homosphere, they do not provide information at lower pressures, particular near and above the homopause, where photochemistry and other energetic processes play a role. The analysis of the stellar occultation experiment [*Festou et al.,* 1981] has provided the preliminary information on the important hydrocarbon profiles and H_2 density profiles. The results are presented in Figure 18. These data are being further analyzed.

Nonauroral precipitation. The Lyα intensity bulge on the dayside suggests that there is a high-energy flux of particles incident on the planet whose deposition pattern is most intense in the region of the Lyα bulge. This flux leaves no emis-

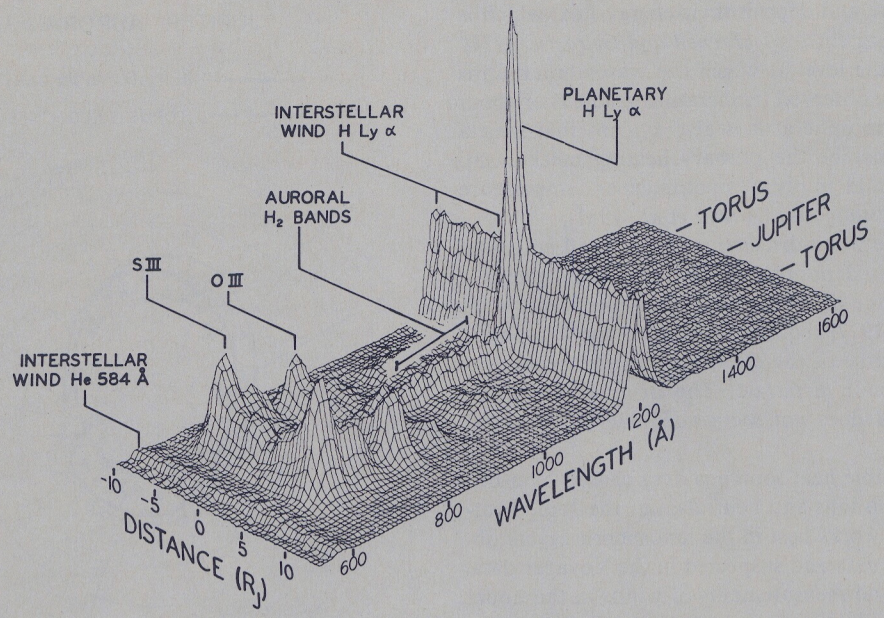

Fig. 21. Ultraviolet spectral-spatial signature of the Jovian system displayed as count rate plotted against space and wavelength. Data acquired over many days were grouped to produce a one-spatial-dimension image of the system. The spatial coordinate has its origin at the planet and is measured in the plane of the rotation equator. The spectrometer slit was oriented roughly perpendicular to this plane. The spatial resolution is 0.5 R_J. Prominent spectral features in the range of 680 to 1000 Å arise from Io's plasma torus; the intensities of these features peak at about ±6 R_J, the radius of the torus. A weak obscuration by Jupiter of a portion of the torus (averaged over many rotations of the torus) is visible near 0 R_J. Radiation from the planet itself is present in the central spike at H Lyα (1216 Å) and in the aurorally excited H_2 Lyman and Werner bands forming the ridge that extends toward shorter wavelengths from the H Lyα peak. Solar H Lyα and He 584 Å radiation resonantly scattered by the interstellar medium form the two ridges running parallel to the space axis. The planetary H Lyα brightness is not shown in its true relationship to the interstellar wind scattering because the planet was much smaller than the UVS slit during these observations from a range of 280 R_J; the slit was filled by H Lyα from the interstellar medium. The true brightness ratio of the planet to the interstellar wind background is a factor of about 30, rather than 2.5 as shown here [*Sandel et al.*, 1979].

sion signature on the nightside, although it may leave its signature on the ionosphere. The nightside Lyα bulge suggests that there is also a flux of particles with a similar deposition pattern but of much softer energy. This flux leaves no (or at most a small) signature on the dayside emission spectrum. The strangest feature perhaps is the day/night behavior of the particle precipitation which gives rise to the presence of the H_2 bands. The excitation is not present on the nightside. If these particles are indeed the source of the hot exosphere, then their absence on the nightside may be discernable in the electron density profile. Any model of particle precipitation must explain the above features of the EUV dayglow and nightglow spectrum.

e. Jupiter's Aurora

The discovery and preliminary analysis of aurora near the poles of Jupiter was reported by *Broadfoot et al.* [1979] and *Sandel et al.* [1979]. Emissions from atomic and molecular hydrogen (Lyα and H_2 Lyman and Werner bands) are excited by electrons penetrating the atmosphere. The integrated intensity in these emissions exceeds 100 kR and implies that 1.2×10^{13} W is supplied to the auroral zones by precipitating electrons. The study of the aurorae can provide unique information for understanding the magnetosphere and its interaction with the atmosphere of the planet. The spectrum of the auroral emission shown in Figure 19 contains the signature of the atomic and molecular hydrogen distributions in the atmosphere, as well as information about the energy spectrum of the exciting electrons. The morphology of the aurorae, including their location on the planet and their spatial (especially longitudinal) and temporal variations, is clearly linked to the structure of the magnetosphere, and very probably to Io's plasma torus.

Preliminary analysis of the data indicated that the equatorward boundaries of the auroral zones corresponded closely to the magnetic projection of Io's plasma torus onto the atmosphere. The finding has been generally confirmed by more detailed analysis, although there may be departures at certain longitudes. Figure 20 shows one example of the analysis using the tip of the UVS slit as a probe to locate the position of the aurora. This map was derived from the Voyager 2 post-encounter north-south map. In this sequence, the UVS slit was scanned repeatedly from north pole to south pole as Jupiter rotated beneath the spacecraft. The slit was almost exactly north-south. The equatorward boundary of the auroral emission can be located by noting the position of the poleward end of the slit when the auroral emission moves into or out of the slit. The precision of the measurement is reduced by the fact that the aurorae are near the polar limbs, so a small uncertainty in slit position corresponds to a relatively larger uncertainty in the latitude of the poleward end of the slit. Although the coincidence of the equatorward boundary of the aurora and the torus map is fairly good in this example, other similar experiments show larger differences in their positions. These differences emphasize the importance of understanding longitudinal magnetospheric asymmetries and their relation to the aurora. Because of the high latitude of the aurora, it is difficult to define the poleward extent of the emitting region. At least at some longitudes, the width of the auroral zones appears to be comparable to the 6000-km width of the slit.

Also present are strong longitudinal variations in the appar-

ent surface brightness of the aurora. Observations by both Voyager 1 and Voyager 2 show that the H_2 band emission in the northern hemisphere has a pronounced maximum in brightness near a longitude of 210°W (System III, 1965). An important question concerns whether this longitudinal structure represents a real difference in surface brightness and hence in precipitating particle fluxes. Another possibility is that the brightness variation is induced by differing absorption path lengths through the atmosphere to the auroral emission source. In the latter case, the shortest path length (and apparently brightest aurora) would occur where the torus mapping dips closest to the equator, i.e., near 170°W in the northern hemisphere. Since this is fairly close to the longitude of the maximum brightness, careful spectral analysis of the auroral emissions and modeling of their transmission through the atmosphere is essential to distinguish between the two possibilities with certainty.

Although the longitudinal structure was roughly the same at the two encounters, the apparent surface brightness of the most intense regions of H_2 emission in the north was about twice as great during the Voyager 1 encounter as the same regions during the Voyager 2 encounter. These bands remain approximately constant in brightness during several days about each encounter. These facts suggest a long-term temporal change in the auroral excitation process. In view of the suggested close connection between the auroral activity and the plasma torus [*Thorne and Tsurutani,* 1979], understanding these temporal effects is particularly important. The changes measured by *Clarke et al.* [1980] using IUE represent a much higher level of variability than deduced from the Voyager measurements to date. The long time base of effectively continuous Voyager data spanning at least 6 months will be examined for similar changes.

It is certain that the polar aurora and its apparent longitudinal variation exist as entities separate from the instantaneous position of Io's flux tube, the 'Io hot-spot' previously detected in Copernicus observations of the Jovian polar region [*Atreya et al.,* 1977]. The hot-spot has not yet been specifically identified in the Voyager UVS data. These data can be used as a critical test of the magnetic anomaly theory of the Io-related hot-spot [*Dessler and Chamberlain,* 1979] which predicts greatly enhanced emission when the foot of Io's flux tube falls in a region of enhanced ionospheric conductivity.

4. The Io Plasma Torus

a. *Introduction*

Observations of EUV radiation from the Jupiter system beginning shortly after launch in late 1977 have shown the presence of strong emission in species other than atomic hydrogen. Most of the atomic emission lines identified in the spectrum (500–1700 Å) arise in the plasma torus at the orbit of Io. The presence of such emitting species as S III, S IV, and O III [*Broadfoot et al.,* 1979; *Shemansky,* 1980*a*] came as a surprise, since ground-based observations of plasma emissions had indicated plasma temperatures too low ($T_e = 2 \times 10^4$ K) to provide measurable quantities of species above the first ionization level. Subsequent events have shown that the analyses of the ground-based observations were certainly correct, but we now realize that the torus had a radially differentiated bimodal character with an undetected hot outer region. The hot outer plasma is of considerable importance to Jupiter's magnetosphere, since it transports most of the energy in the torus system. In the following subsections we discuss the advances that have been made in understanding of the torus processes based on the EUV observations in combination with other complementary experiments.

b. *Morphology*

The in situ measurements of the Voyager plasma science experiment [*Bridge et al.,* 1979] coupled with the EUV and ground-based observations have now established that the plasma torus is in a bimodal quasi-steady-state, with an outer region centered at ~5.9 R_J having an effective electron temperature of $T_e \simeq 10^5$ K and an inner region centered at ~5.3 R_J with $T_e = 2 \times 10^4$ K. The EUV data suggest that the plasma has been in this condition since at least late 1977; the early observations of Jupiter show measurable torus emission. There is a strong suggestion that the torus may have been significantly different at the time of Pioneer 10 encounter in late 1973 [*Broadfoot et al.,* 1979; *Judge et al.,* 1976]. Ground-based optical observations had been confined to the cool emitters of the inner torus up to the time of Voyager 1 encounter [see *Shemansky,* 1980*b*, and references therein]. Thus there appears to be no available observational evidence on the hot plasma torus between Pioneer 10 encounter and late 1977, and very little is known of its long-term temporal morphology. The spectral content and intensity of the EUV plasma emitters in the several months period surrounding Voyager 1 encounter averaged over ~10-hour periods is reasonably constant up to about day 160/1979. After that time the hot torus emissions according to Voyager 2 observations show a cooling trend accompanied by some changes in spectral content and increased intensities up to the time of Voyager 2 encounter [*Sandel et al.,* 1979].

The spatial distribution of the hot EUV plasma is that of a full continuous torus with a radius of symmetry of 5.9 R_J and a cross-sectional half width of 1 R_J both in the magnetic plane and perpendicular to the plane. Although factor of 2 variations in intensity are observed, presumably due to spatial nonuniformity in the plasma, the hot torus shows no particular dependence on magnetic longitude. This is in sharp contrast to the cool inner torus, which shows a strong (order of magni-

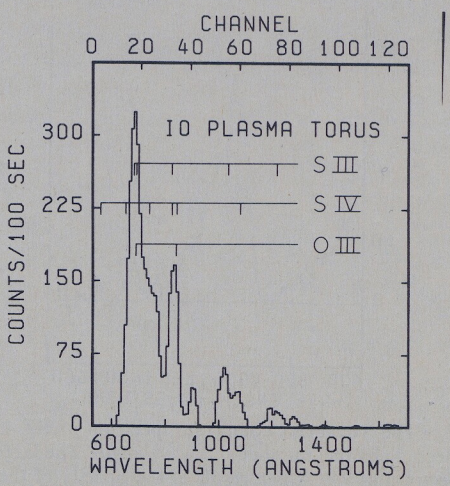

Fig. 22. Spectrum of the Io plasma torus obtained at 5.9 R_J from Jupiter center on day 60/ 1979, 1800–2030 GMT. The satellite Io was in the field of view during the observation, but no emission related to the position of Io has been detected in the EUV spectra (see text). Some lines of identified species are indicated in the spectrum. The feature at 685 Å is dominated by S III and has a brightness of 200 R [*Broadfoot et al.,* 1979].

TABLE 2. Analysis of the Io Plasma Torus Spectrum of the Voyager 1 Encounter Period

Species	Density, cm^{-3}
O II	49
O III	336
O IV	<17
S II	44 ± 22
S III	160
S IV	216
S V	≤11
K III	≤80
e	1850

Estimated average number densities in the dense region of the hot plasma, based on the analysis of the spectrum in Figure 22 [*Shemansky and Smith,* 1981]. The electron temperature in the analysis was 8.0×10^4 K with an inclusion of 1×10^6 K electrons in a <1% mixing ratio. The approximate relative number densities [O]/[S] ≃ 1.0.

tude) magnetic longitude dependence and instabilities in shape and position relative to the magnetic plane [*Pilcher,* 1980; *Trafton,* 1980; *Trauger et al.,* 1980]. Figure 21 shows the EUV image of the Jupiter system, indicating the distribution of the strong sulfur and oxygen emission. The figure is illustrative of the spatial uniformity of the EUV emitters, which show no measurable dependence on magnetic longitude [*Sandel,* 1980]. Observations with the Voyager UV spectrometer show no measurable Io-associated EUV emissions [*Broadfoot et al.,* 1979]. This result is of particular importance to the question of mass loading of the torus in the near vicinity of Io, as discussed below.

c. *Plasma Composition*

The species identified in the Voyager EUV spectrum with varying degrees of certainty are S III, S IV, S V, O II, O III, and K III [*Broadfoot et al.,* 1979; *Shemansky,* 1980*a*; *Shemansky and Smith,* 1981]. These species do not necessarily account for all of the features present in the spectra, and in particular, a persistent feature at 900 Å has not been satisfactorily

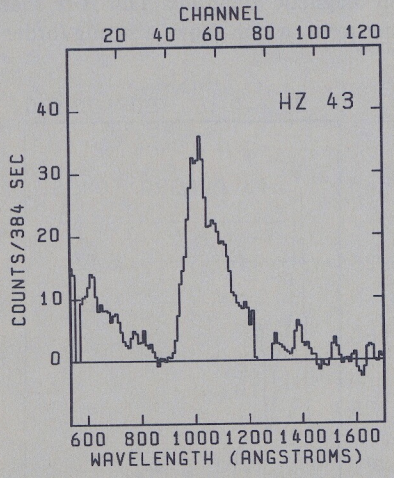

Fig. 23. The Voyager 2 count rate spectrum of HZ 43 as a function of spectral channel number and wavelength. The large decrement in the spectrum at 900 Å is a result of the opacity of the interstellar medium. The absorption features in channels 51 and 56 are due to the Lyman γ (976 Å) and Lyman β (1025 Å) lines, respectively, in HZ 43. We have discarded the data in channels 3 and 4 because of low sensitivity, and in channels 76–81 because of a large Lyα foreground correction, which causes flux estimates to be unreliable in these channels. Longward of 1400 Å, HZ 43 is below the detection threshold of the instrument.

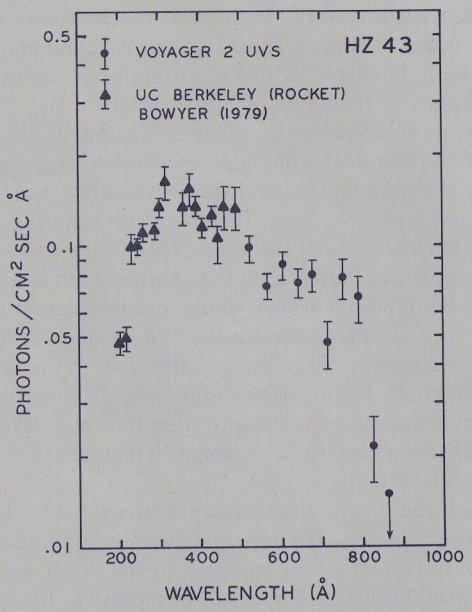

Fig. 24. The EUV spectral flux for HZ 43 from combined Berkeley [*Bowyer,* 1979] and Voyager 2 observations. The absolute calibration was done independently. The agreement between the two calibrations at 500 Å is quite good. The decreasing flux towards 900 Å is due to the increasing absorption cross section of HI in the interstellar medium. The data point just shortward of 900 Å is an upper limit on the flux. The Voyager data points represent 4-channel averages.

identified. Figure 22 shows a spectrum typical of the Voyager 1 encounter period. The analysis of the spectrum in general is conducted through the synthesis of the emission spectrum using model calculations of collisional equilibrium within each subspecies. Four analyses of the spectrum have been published to date [*Broadfoot et al.,* 1979; *Shemansky,* 1980*a*; *Strobel and Davis,* 1980; *Shemansky and Smith,* 1981]. Differences in the results are due mostly to advances in our knowledge of collision strengths that have taken place in the past year. The most recent analysis [*Shemansky and Smith,* 1981], which takes into account a nonthermal equilibrium in electron energy distribution [*Scudder et al.,* this issue], gives the ion densities and upper limits shown in Table 2. These densities refer to the average over the central 1-R_J region of the hot torus as represented by Figure 22. The *Strobel and Davis* [1980] analysis, which also applies a nonthermal electron energy distribution, differs somewhat from the result given in Table 2 mostly because of the use of what are now considered to be inaccurate collision strengths for the S IV system and a lower assumed temperature. Part of the analysis of *Strobel and Davis* [1980] depends on the assumption of a high diffusive loss rate. The more recent analyses by Strobel [*Pilcher and Strobel,* 1981] and *Shemansky and Smith* [1981] show better agreement in regard to estimated population densities. The estimated electron temperatures for the results given in Table 2 are $T_e = 8.0 \times 10^4$ K with an inclusion of <1% $T_e = 10^6$ K electrons. The mixing ratio of hot electrons is somewhat uncertain, but the analysis of the EUV spectrum cannot tolerate ratios of $T_e = 10^6$ K electrons above 1% [*Shemansky,* 1980*b*], and the effect on the ion number densities obtained from the spectral analysis is small.

Sulfur and oxygen appear to be the dominant ions in the torus. Apart from a possible identification of K III, no other species have been identified to date in the EUV spectra, although not all of the spectral features have been accounted

for. Upper limits in Si II, Si III, Si IV, Ar II, C III, and H I have been estimated by *Shemansky* [1980*a*]. The plasma science experiment has established that the dominant species have a mass per unit charge corresponding to oxygen and sulfur ions [*Sullivan and Bagenal,* 1979] and has in addition identified trace amounts of Na II and heavier molecular species. The analysis of the plasma science data [*Sullivan and Bagenal,* 1979] also implies the presence of only trace amounts of H II, although direct measurement within the hot torus was not possible.

d. Mass Loading and Diffusion Loss

The rates of mass loading and diffusion loss are directly related quantities that are of great importance to the determination of the source of radiative energy and the role of the torus in the Jupiter magnetosphere. Information on these quantities is contained in various aspects of the radiated spectrum of the torus, and the Voyager EUV data in particular are playing an essential role in providing direct quantitative estimates. Limits to mass loading can be obtained from measurements of the partitioning of ion species, as described in the following discussion.

A given subspecies, S III say, generally has an excited state population relaxation time orders of magnitude shorter than the ion diffusion loss times that one may reasonably expect in the torus. The spectrum of a particular subspecies is almost always close to collisional equilibrium and therefore does not carry the signature of diffusion loss rates. However, the relative populations of the subspecies derived from the spectral analysis are affected by diffusion loss rates if ionization and recombination lifetimes are comparable to the diffusion loss times. Thus our expectations are that subspecies will be in collisional equilibrium, but the partitioning of species will not necessarily show a collisional equilibrium distribution. The effect of diffusion loss on a plasma in statistical equilibrium is to produce a cool ion distribution, a S II:S III:S IV:S V, for example, that is not in collisional equilibrium with the electron energy distribution. Thus spectroscopic observations can provide a measure of the diffusion loss rate. If large quantities of S II and O II were shown to be present in the hot torus in a 10^5-K electron gas, then one could conclude that the loss rate by diffusion was large. If, on the other hand, the ions were partitioned in a distribution close to expectation for a gas in collisional ionization equilibrium, then one would expect a very long diffusion loss time, possibly controlled by recombination to neutral atoms. The analysis which provides the distribution estimate shown in Table 2 indicates that the real ion distribution of the plasma lies between the extremes. The solution of the steady state equations of ion partitioning, taking into account a nonthermal electron distribution, leads to an estimate of diffusion loss time of the order of 100 days [*Shemansky,* 1980*b*]. The accuracy of the result depends on a number of factors that are not discussed in detail here, but the most important result determining a long diffusion loss time is the indication that S II and O II are present, on the average, in only small relative quantities in the hot torus. This spectroscopic result must still be reconciled with the in situ plasma

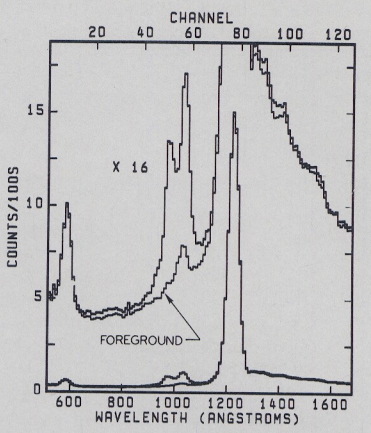

Fig. 26. Raw Cygnus Loop spectrum obtained in the mean direction $\alpha = 311.9°$, $\delta = 31.4°$ after correction for fixed pattern noise, plotted with the foreground spectrum composed mostly of resonance scattered solar radiation in the intervening medium (see text). The integration time is approximately 5×10^5 s. The obvious line structure in the spectra is superposed on signal components composed of weak diffuse galactic emission, energetic particle noise and internally scattered radiation.

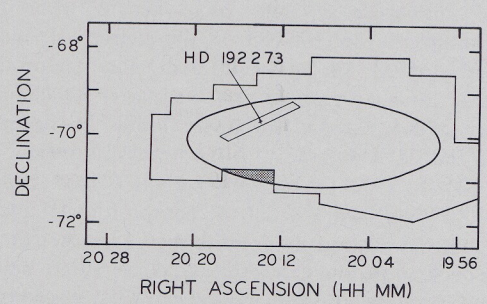

Fig. 25. The irregular polygon is the area searched by the Voyager 2 UVS. The ellipse is the error boundary of the *Cash et al.* [1978] observation. The UVS FOV is indicated by the small parallelogram centered on HD 192273. The portion of the Cash et al. error box excluded from the Voyager 2 search is indicated by the stippled region. These observations established an (2σ) upper limit of 3.2×10^{-2} photon cm^{-2} s^{-1} $Å^{-1}$ for any EUV source in the 513- to 754-Å band within 95% of the Cash et al. error box. In addition, no FUV (911 to 1200 Å) sources, other than HD 192273, were found down to a sensitivity threshold of 0.08 of the brightness of HD 192273.

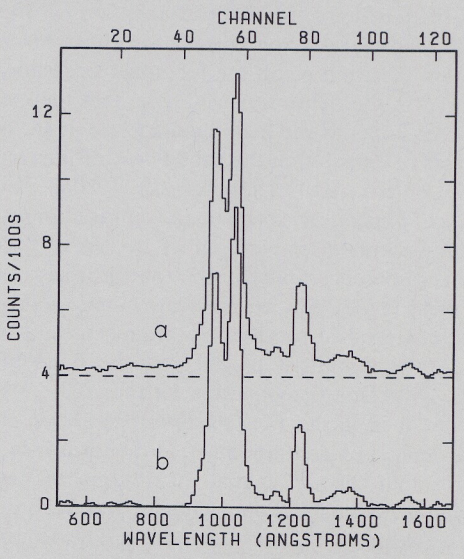

Fig. 27. (*a*) The Cygnus Loop spectrum after subtraction of the foreground spectrum of Figure 26. The spectrum contains no contaminating signal other than internally scattered radiation. (*b*) The Cygnus Loop spectrum after final reduction. The spectrum is the product of the scattering matrix operator and the spectrum of (*a*). The scattering matrix operator removes internal instrumental scattering of the incident radiation and second-order lines. Tentative line identifications are given in the text.

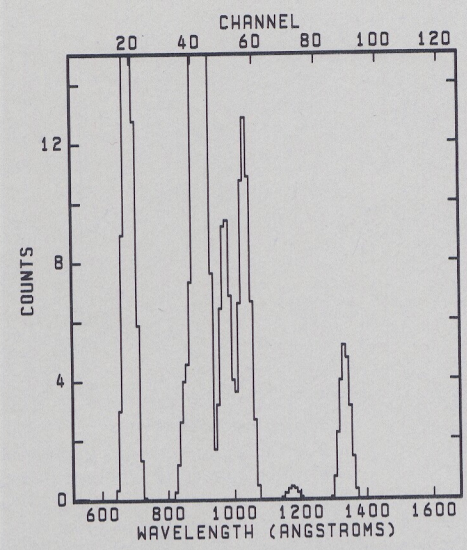

Fig. 28. Model calculation with C II and C III in collisional equilibrium at an electron temperature of 10^5 K, showing line features which correspond to structure in the spectrum of Figure 27. The model does not include a correction for extinction in the interstellar medium, and the lines shortward of 912 Å would be entirely removed by continuum absorption. No attempt has been made to fit the model to the data, and the synthesis serves only as an illustration of the method of analysis of the UV spectrometer data [cf. *Shemansky et al.*, 1979*b*].

science measurements which showed substantial numbers of particles with the mass per charge ratio of 32 in the hot region of the torus [*Bagenal et al.*, 1980].

The particular spectrum of the torus shown in Figure 22 was taken when Io was in the field of view and near elongation. The side of the satellite bombarded by the torus plasma was in view. The spectrum is the same when Io is out of the field of view. If one makes the reasonable assumption that Io is the ultimate source of ions maintained in the plasma, the source processes which occur near the satellite should emit radiation characteristic of the production of ions in proportion to the mass loading rate. Source emissions have not been detected in this spectrum or on the few other occasions that Io has appeared in the field of view. These data then allow the calculation of limits to the mass loading rate at Io, based on known yields of emission in the production of ions from electron impact on S I and O I [*Shemansky*, 1980*b*]. Thus if the only source of ionization is oxygen and sulfur atoms, the mass loading rate is limited to the order of 10^{27} ions s^{-1}. We note that there is some uncertainty in the source process, since the products yield of $e + SO_2$ is not a measured quantity [*Shemansky*, 1980*b*] and dissociation to atomic species has been assumed as the dominant product on the basis of energy thresholds. This result is compatible with the 100-day diffusion loss time obtained in the analysis described above. However, the results depend on assumptions that the torus is in a quasi-steady-state, that the ion spatial distribution in the central dense region is reasonably homogeneous, and that most of the ions are created from O I and S I near Io. The accuracy with which these assumptions hold controls the accuracy of the analysis. These results indicating fairly long diffusion loss times and low mass loading rates are potentially in conflict with the plasma science measurements which suggest that on some occasions the ions in the region of the magnetosphere outside the Io torus may not be corotating [*Bridge et al.*, 1979]. *Hill* [1980] estimates a mass loading rate of 10^{28} particles s^{-1} with mass of SO_2 on the assumption that the rotational slippage observed by *Bridge et al.* [1979] occurs continuously. Other work by Siscoe and coauthors [see *Shemansky*, 1980*b*] suggests that the disequilibrium in the ion and electron temperatures in the hot torus may be controlled by a high diffusion loss rate. However, this theory requires most of the ionization to occur near Io, and the spectroscopic results described here tend to set a rather severe limit on direct mass loading.

e. *Energy Balance*

The EUV observations have established that the hot outer plasma torus transports most of the energy of the system. The rate of energy loss by radiation from the hot torus is estimated to be $\sim 3 \times 10^{12}$ W based on calculations of collisional equilibrium within each ion species of sulfur and oxygen [*Broadfoot et al.*, 1979; *Shemansky*, 1980*b*]. The half-life of the torus emission would be ~20 hours if the energy source were removed. The input of energy must therefore be at least 3×10^{12} W and continuous on the time scale of 20 hours. Possible sources for the energy depend on the estimated mass loading rate. If it is assumed that energy is supplied by the acceleration of newly formed ions, then Io must supply at least $\sim 2 \times 20^{28}$ ions s^{-1} of oxygen or sulfur. The spectroscopic data seem to indicate that the mass loading rate is less than this value and the energy must then arise through interaction with Jupiter's magnetosphere. Observations of >7-meV sulfur and oxygen ions in the vicinity of the torus [*Vogt et al.*, 1979] suggest that acceleration mechanisms may not be well understood.

f. *Source Processes*

There appears to be little doubt that Io is the major source of particles in the torus. Our knowledge of the details of how the particles enter the torus converted to sulfur and oxygen is limited. The dominant atmospheric source particle for the torus is SO_2, according to measurements by the Voyager IR experiment [*Pearl et al.*, 1979] and related calculations [*Johnson et al.*, 1979; *Kumar*, 1979]. The dominant dissociative and ionization process is likely to be electron impact, but product branching, rate coefficients, and kinetic energy of the dissociated particles are mostly unknown. The majority direct ionization channels are SO_2^+ and SO^+, and trace amounts may have been detected in the torus [*Sullivan* and *Bagenal*, 1979]. The number density ratio of oxygen to sulfur in the torus, assuming atmospheric SO_2 as the source, depends on the branching of the ion and neutral dissociation products. The expected ratio is therefore not necessarily [O]/[S] = 2.0 [*Shemansky*, 1980*b*; *Strobel and Davis*, 1980]. The estimated value from the EUV data around the time of Voyager 1 encounter is [O]/[S] $\simeq$ 1.0 (Table 2). We emphasize that the deviation of the [O]/[S] ratio from the composition of the SO_2 molecule does not necessarily point to a source other than atmospheric decomposition. Our ability to discriminate between surface sputtering and atmospheric sources will depend on developments in our knowledge of $e + SO_2$ physical chemistry.

5. SATELLITE ATMOSPHERES

a. *Callisto Airglow Observations*

Airglow observations of the Jovian satellites were designed to search for bound atmospheres. Atomic species can be identified by their characteristic airglow emissions arising from resonance scattering of the solar flux. Species that scatter effi-

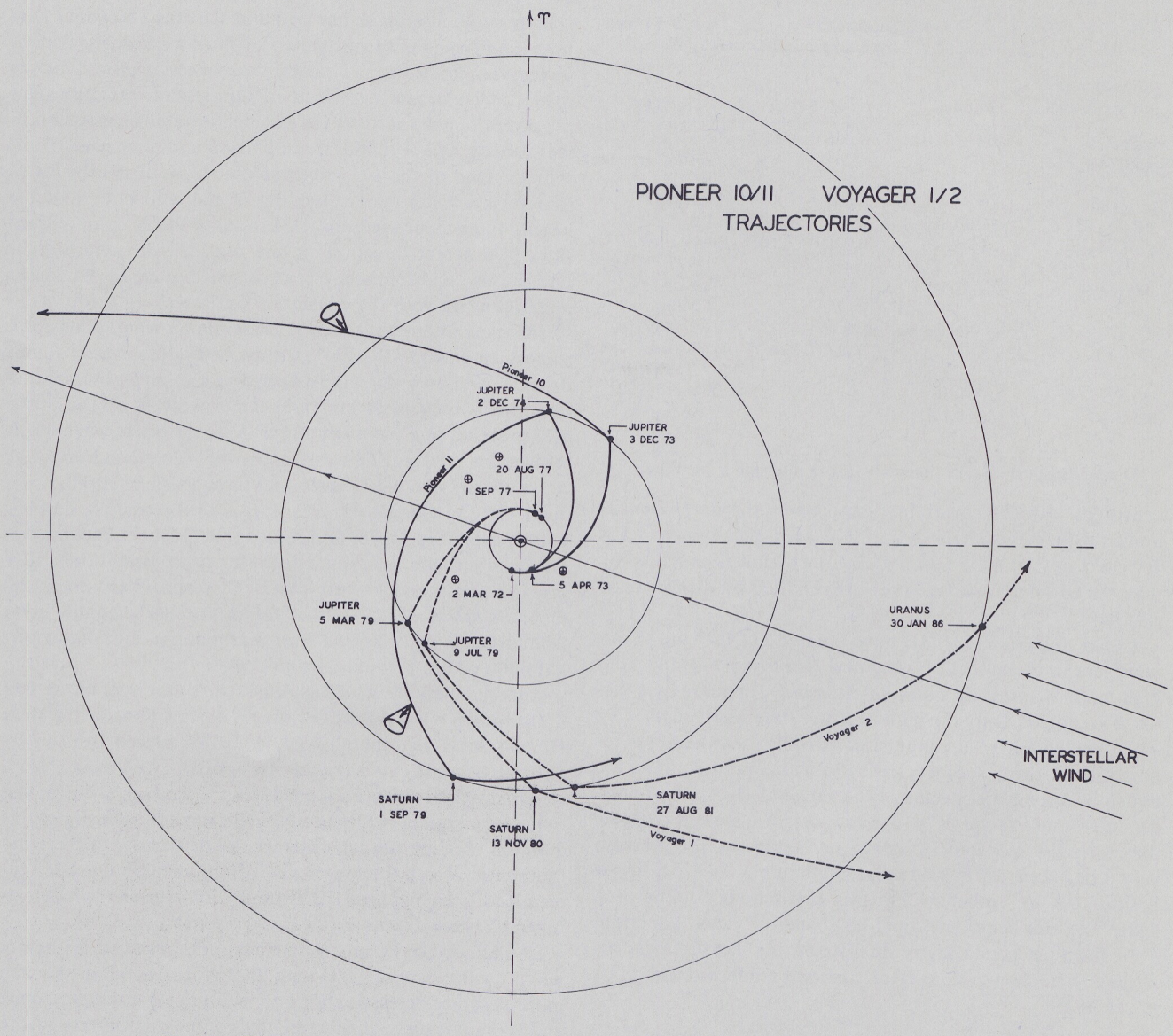

Fig. 29. The trajectories of the Pioneer and Voyager spacecraft as they depart from the solar system.

ciently in the wavelength range of the UVS are H, He, O, and C. Although airglow observations were made for all the Galilean satellites, most were compromised by the high radiation-noise rate in the instrument detector. The most favorable combination of observing geometry and low radiation-noise occurred during Voyager 1 observations of Callisto.

Species in a gravitationally bound atmosphere can be most easily detected just off the bright limb of the satellite. Here the column density reaches its peak, and except for hydrogen and helium, there is little competing sky background emission. No emissions from the vicinity of Callisto have been positively identified. An upper limit of 150 R on the atomic oxygen emission at 1304 Å corresponds to a surface density of less than 2×10^6 cm^{-3}. Upper limits on the surface densities of bound atmospheres of other species are [He] $< 7 \times 10^4$ cm^{-3} and [C] $< 10^8$ cm^{-3}. The data suggest that atomic hydrogen may be present, but the analysis is complicated by the high radiation-noise and brightness of the Lyα sky background. Further study of the question of the presence of H is in progress.

Another technique for determining the composition and density of an atmosphere is the measurement of its absorption, rather than scattering, characteristics. This can be done by observing the occultation of a star by the body. Since normal stars show no flux at wavelengths less than 912 Å, species which absorb only below this wavelength cannot be detected by stellar occultation. However, many species of interest, including O_2, H_2O, CO_2, and CH_4 have appreciable absorption cross sections in the appropriate wavelength range and are therefore detectable by this technique.

b. *Ganymede Stellar Occultation*

The UVS observed the moderately bright star κ Centauri as it was occulted by Ganymede (B. R. Sandel, manuscript in preparation, 1981). As seen from the spacecraft, the star moved almost exactly across a diameter of Ganymede. Removal of radiation background and modulation due to spacecraft attitude control motions from the signal leaves a clearly defined occultation signature having a time resolution of 0.32 s. The signature shows no evidence for atmospheric absorption. For a number of possible atmospheric constituents we have calculated upper limits on the surface density that are

TABLE 3. Densities in Nearby Interstellar Medium Deduced From H 1216 Å and He 584 Å Sky Background Observations

Spacecraft Observations	n_H, cm^{-3}	n_H, cm^{-3}	Reference
Mariner 10 (RCM 1, 3, 4)	0.04 ± 0.015	0.006 ± 0.002	*Kumar and Broadfoot* [1979]
Mariner 10 (RCM 7)	0.04 (+0.03, −0.02)	0.008 ± 0.005	*Ajello* [1978]
Apollo-Soyuz	···	0.0089 ± 0.005	*Freeman et al.* [1977, 1979]
Copernicus	0.01–0.04*	···	*Blum and Fahr* [1976]
STP 72-1	···	0.008–0.020	*Meier* [1977]
STP 72-1	···	0.009–0.024	*Weller and Meier* [1974]
Ogo 5	0.03–0.12	···	*Thomas* [1972]
Ogo 5	0.08–0.12	···	*Bertaux et al.* [1972]

*Derived from the ionization state of the interstellar medium.

consistent with the constraints imposed by the data. Density limits for species such as O_2 and H_2O are typically near 1.5×10^9 cm^{-3} or 2×10^{-8} mbar. This upper limit is much lower than the 10^{-3}-mbar surface pressure reported by *Carlson et al.* [1973].

Kumar and Hunten [1981] have pointed out that the O_2 atmosphere in the model of *Yung and McElroy* [1977] has both high- and low-pressure states differing in O_2 pressure by a factor of about 10^5. Only the high-pressure state was discussed by Yung and McElroy in connection with the measurements reported by Carlson et al. According to Kumar and Hunten, the switch between states occurs over a range of H_2O partial pressure of about a factor of 2. The low-pressure state is compatible with the Voyager observations, since the O_2 pressure would be about 1.5×10^{-9} mbar, well below the UVS upper limit of 2×10^{-8} mbar. Although a single body could switch states, the time required would be about 10^5 years. Therefore even given the possibility of dual states, the measurement reported by Carlson et al. is clearly incompatible with the UVS upper limit.

6. VOYAGER ASTRONOMICAL OBSERVATIONS

a. *Introduction*

The Voyager ultraviolet spectrometers were designed primarily to study the upper atmospheres of the outer planets, but they also possess several unique advantages which make them useful astronomical tools. The principal advantage of the Voyager instruments is their spectral range (500–1700 Å). With the advent of the astronomical satellites such as OAO 2, TD1, IUE, etc. the region of the spectrum longward the MgF_2 cutoff at 1150 Å has been well surveyed. This is not the case for the region between 1200 Å and the Lyman limit at 912 Å. Copernicus has explored this region at very high spectral resolution but largely in terms of relative flux and brighter stars. Voyager can make observations of absolute stellar flux in this region to below visual magnitude 12 for high-temperature objects. The opening of the extreme ultraviolet (EUV) region between the soft X ray (100 Å) and the Lyman limit at 912 Å to astronomical exploration was begun only recently with the discovery of EUV sources [*Lampton et al.*, 1976; *Margon et al.*, 1976] during the Apollo-Soyuz mission. It is in this region, between 500 and 900 Å, where the Voyager instruments are making some of their most important contributions to observational astronomy.

During the interplanetary cruise phase of the Voyager mission, the ultraviolet spectrometers on both spacecraft have observed various stellar and nonstellar sources of ultraviolet radiation. The results described in this section are part of a program designed to look for extreme ultraviolet emission in the 500- to 900-Å band from known and suspected EUV sources. One of the objectives of the study of nearby EUV sources is a better understanding of the distribution of the nearby interstellar medium. Determining the H column densities in different directions is one way to gain some insight into the size and frequency of occurrence of clouds of denser material along with the density of the intercloud medium.

The most important factor in determining whether or not a star which emits in the EUV will be detectable is the column density of intervening H between the star and observer. As little as 3×10^{18} atoms/cm^2 of H can provide an optical depth of 5 to stellar flux observed at 513 Å, the shortest wavelength reached by Voyager. This column density corresponds to a distance of only about 10 parsec (pc) through an interstellar medium with an average H density (n_H) of 0.1 cm^{-3}, a number *McClintock et al.* [1978] find reasonable for the immediate solar neighborhood. It is quite clear, however, from other EUV measurements and Copernicus H Lyα absorption measurements [*Cash et al.*, 1979] that the interstellar medium is far from uniform and, in some directions, observations out to perhaps 100 pc are possible.

Another method, which is sensitive to the interstellar medium within ~100 AU of the sun, is observations of the solar He 584 Å, H Lyα, and Lyβ lines backscattered from interstellar He and H entering the solar system. The Voyager UVS observations of these emissions from a vantage point in the outer solar system can be used to determine the density of this material entering the solar system. A comparison of these determinations with the longer path length column densities determined from Voyager EUV source observations will be significant, as we discuss below.

In addition to the interstellar medium, observations of hot white dwarfs between 500 and 1200 Å can be used to make more accurate determinations of their effective temperatures, and by implication, their radii. This is most important at the

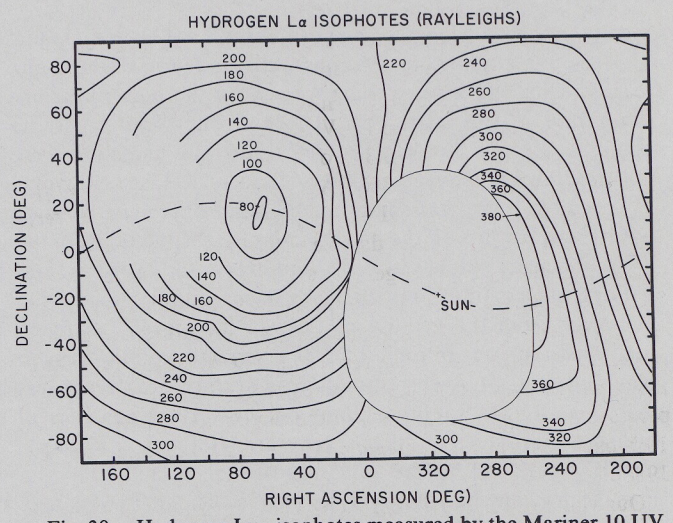

Fig. 30. Hydrogen Lyα isophotes measured by the Mariner 10 UV spectrometer [*Broadfoot and Kumar*, 1978]. The data were collected on January 28, 1974, while the spacecraft was at a heliocentric distance of 0.757 AU and ~60° from the downwind axis. The units are rayleighs.

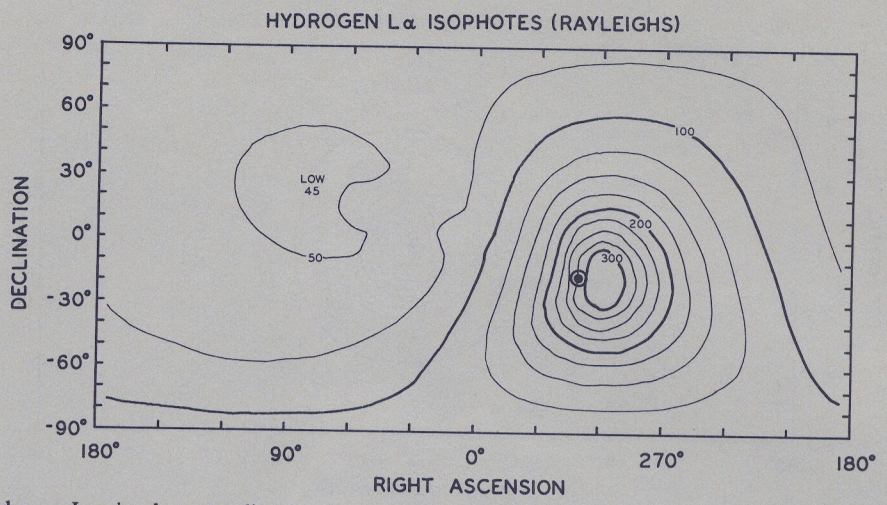

Fig. 31. Hydrogen Lyα isophotes predicted using the model parameters derived from Figure 30 but from an observational position near Jupiter on the Voyager trajectory (see Figure 29). The units are rayleighs.

upper end of the white dwarf temperature scale, where ground-based observations become rather insensitive to temperature (for a review of UV and EUV white dwarf observations, see *Shipman* [1979]).

The following is a brief discussion of each of the individual objects for which some Voyager results are available at this time.

b. Stellar Sources

HZ 43 ($\alpha = 198.5°$, $\delta = 29.4°$). This hot white dwarf was the first observed extrasolar source of EUV emission [*Lampton et al.*, 1976] and has received considerable observational and theoretical attention.

Emission from HZ 43 has been detected in the 500- to 800-Å band with both Voyager spacecraft on several separate occasions. The Voyager 2 HZ 43 observations of January 9 and 10, 1980, reported by B. Holberg et al. (manuscript in preparation, 1981) (Figure 23) provide the first measurements of two previously unobserved regions of the spectrum: the 500- to 800-Å EUV region and the 900- to 1200-Å far ultraviolet (FUV) region. The EUV observations agree quite well with the rocket results of *Bowyer* [1979] at 500 Å (Figure 24). As the spectrum longward of 500 Å is quite sensitive to the column density of intervening neutral hydrogen (N_H), the Voyager 2 results firmly establish N_H in the direction of HZ 43.

The Voyager 2 EUV and FUV results were combined with existing flux data from HZ 43 at other wavelengths: 200 to 500 Å [*Bowyer*, 1979], 1150 to 3000 Å [*Greenstein and Oke*, 1979], and 1550, 1800, 2200, and 2500 Å [*Wesselius and Koester*, 1978]. From this combined data set it has been possible to obtain a best fit pure hydrogen model atmosphere with an effective temperature of 55,000 K, log $g = 8$, and interstellar N_H of 3.9×10^{17} cm^{-2}. Previously, the broadband Apollo-Soyuz EUV fluxes of *Lampton et al.* [1976] had been used along with model atmosphere fluxes to establish similar temperatures, an upper limit to N_H in the direction of HZ 43 of 2×10^{18} cm^{-2} [*Auer and Shipman*, 1977; *Heise and Huizenga*, 1980].

Our value of 3.9×10^{17} cm^{-2} (N_H) is surprisingly low for an object at the distance (62.5 pc) of HZ 43, as it implies an average line of sight H density of 0.002 cm^{-3} (n_H). Such a result is not entirely unexpected, however. *Anderson and Weiler* [1978] have measured an n_H of 0.003 to 0.007 cm^{-3} from Lyα absorption measurements for HR 1099, a star 33 pc distant. Observations of two more distant stars, β CMa (213 pc) and ε CMa (179 pc), by *Bohlin* [1975] indicate values of $n_H < 0.01$ cm^{-3}. This Voyager determination of the HZ 43 H column density, together with our measurements and lower limits in the directions of other objects, provides an important probe of the local interstellar medium.

HD 192273 ($\alpha = 303.5°$, $\delta = 69.6°$). This star was suggested by *Cash et al.* [1978] as an identification for a possible EUV source in the constellation Pavo observed during the Apollo-Soyuz mission. Voyager 1 observed the HD 192273 spectrum in the 912- to 1500-Å band and detected no EUV emission [*Barry et al.*, 1980]. The upper limit established with these observations is 1/10 that reported by Cash et al. in the 500- to 750-Å band. On this basis, it was concluded that HD 192273 is probably not the potential EUV source reported by Cash et al. Later observations by Voyager 2 searched 95% of the Cash et al. Pavo EUV source error box and detected no EUV emission above a limit 1/3 that reported by Cash et al. (see Figure 25). Two interpretations of HD 192273 seems possible from its visual spectrum. If HD 192273 resembles a normal B2V star, then its visual magnitude of 8.8 implies its distance is large (~4 Kpc), ruling out any EUV flux. Its high galactic latitude, however, would place it ~2 Kpc above the galactic plane, a very unlikely location for an early main sequence B star. *Shipman and Wegner* [1979] have suggested an alternate interpretation of HD 192273 as a nearby (100–200 pc) evolved mass exchange binary system in analogy with HZ 22. This type of model would be necessary to explain the reported EUV emission. In light of Voyager results a major motivation for this interpretation of HD 192273 is removed. However, the problem of the location of HD 192273 above the galactic plane remains.

HD 149499 B ($\alpha = 248.6°$, $\delta = -57.4°$). This star was detected as abnormally bright during the Skylab UV survey and has been interpreted as being due to a hot white dwarf companion to the K 0 V primary [*Parsons et al.*, 1976]. IUE observations [*Wray et al.*, 1979] indicate an effective temperature in the range of 85,000 K, making it one of the hottest white dwarfs known. If the distance estimates of 30 to 40 pc of *Wray et al.* [1979] are correct, then EUV emission from this object would be a defininte possibility. HD 149499B has been observed by both Voyager spacecraft, and the Voyager 1 obser-

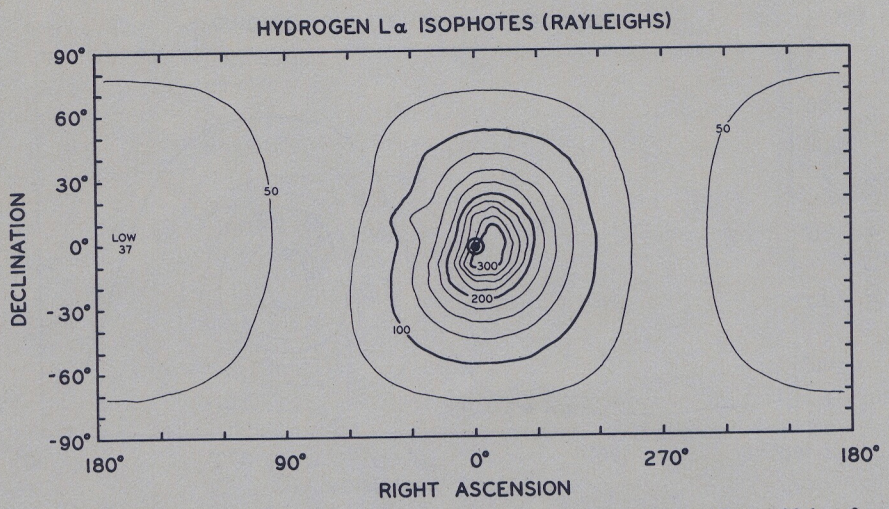

Fig. 32. Hydrogen Lyα isophotes predicted using the model parameters derived from Figure 30 but from an observational position near Saturn on the Voyager trajectory (see Figure 29). The units are rayleighs.

vations indicate no detectable EUV emission. From this, it is possible to establish a preliminary lower limit of 1×10^{18} cm^{-2} for N_H in the direction of HD 149499B. This result can most likely be improved upon by further analysis and the Voyager 2 results.

HR 1099 (α = 53.55°, δ = 0.43°). HR 1099 is a bright nearby (d = 33 pc) RS Canum Venaticorum binary system. On the basis of soft X ray detections [*Walter et al.,* 1978] the low reported N_H of 5.1×10^{17} cm^{-2} [*Anderson and Weiler,* 1979], and an analogy with the spectral distribution of solar flares, it is expected that EUV flare emission would be detectable with Voyager.

An entire month of Voyager cruise observations was devoted to HR 1099. These observations were undertaken in coordination with ground-based radio and optical observations in hopes of a simultaneous flare observation. During the Voyager observing period, no flare activity was observed in the ground-based data. The quick look samples of the Voyager data which have been analyzed show no signal at any wavelength (as would be expected for HR 1099 in its quiescent state). Although unsuccessful, this observation demonstrates the usefulness of Voyager's ability to remain pointed at a target for long periods of time. For observations of flare stars and irregular variables, extended monitoring is often a very fruitful technique.

c. *The Cygnus Loop Supernova Remnant*

Voyager EUV observations have provided the first measurements of the Cygnus Loop supernova remnant (SNR) at wavelengths below 1100 Å [*Shemansky et al.,* 1979*b*]. The SNR has been studied extensively over the years [*Parker,* 1967; *Chamberlain,* 1953]. The object shows chaotic structure in optical filaments and has an overall diameter of ~3.4°, at a distance of 770 pc. No known exciting star has been detected, and thermal energy is consequently assumed to arise in the interaction of the expanding shell with the interstellar medium. Observations of the bright optical filaments show characteristic temperatures from 10^4 to 10^5 K. More recent observations have established the presence of higher-temperature reactions producing soft X rays, emission lines of the more highly ionized species, and other characteristics of fast shock waves [*Rappaport et al.,* 1979; *Woodgate et al.,* 1977; *Raymond et al.,* 1980*a*]. The SNR therefore has a complex structure showing the presence of significantly differing shock velocities. Measurements in the EUV are of particular importance for the study of SNR's, since primary high-temperature shock processes are more easily measured in this region of the spectrum, and some species such as carbon and silicon, which are important to research on the role of interstellar grains in the shocked gas, do not have measurable lines at longer wavelengths.

The Voyager 2 UVS has observed Cygnus Loop on three occasions widely separated in time. Spectra of loop objects NGC 6995 and NGC 6992 were obtained during November 1977 and April 1978. A preliminary analysis of the earlier of these observations has been published [*Shemansky et al.,* 1979*b*]. Recent observations in December 1979 and early 1980 are the most extensive. These recent data will be used to construct tomographs of the entire SNR structure in 500- to 1700-Å radiation by using an established method of utilizing spacecraft pointing system drift and limit cycle motion (see Figures 7 and 21). Figure 26 shows a high-quality spectrum obtained from the recent observations in the mean direction α = 311.9°, δ = 31.4°. The short-wavelength features and some of the longer-wavelength features are common to the spectra obtained in the direction of NGC 6995 and 6992 at ~α = 313.7°, δ = 31.3° [*Shemansky et al.,* 1979*b*]. Although detailed model calculations have not been made, tentative identification of some of the features are C III, 977 Å; C II, 1037 Å; He II, 1080 Å; C II, 1175 Å; C II, 1335 Å; O IV, S IV; Si IV, 1400 Å; C IV, 1550 Å; and He II, 1640 Å. The spectrum in the long-wavelength region is similar in some respects to the recent IUE spectrum obtained by *Raymond et al.* [1980*b*] at another location on the SNR. The feature in Figure 27 at 1225 Å has not been identified, although *Shemansky et al.* [1979*b*] have suggested that it may correspond to a dissociative transition in H^-. The recognition of a feature at 1225 Å in the spectrum is illustrative of the stability of the EUV instrument, since the line appears only after subtraction of the sky background spectrum containing the bright Lyα line at 1216 Å (see Figure 26). The 1225-Å feature appears persistently at other locations in the SNR [*Shemansky et al.,* 1979*b*]. Figure 28 shows a model calculation of collisional equilibrium in C II and C III at an electron temperature of 10^5 K, which may be compared to the observed spectrum. The model contains no correction for extinction and is shown only to illustrate the analysis procedure;

lines shortward of 912 Å are entirely removed by hydrogen continuum absorption. Further work on these high-quality data in the production of EUV images of the loop structure and in comparison with model calculations of shock-generated radiation is expected to provide a significant advance in our understanding of SNR's.

7. EUV Sky Background

a. Interaction of the Solar Wind With the Interstellar Medium

The solar wind is our prototype of stellar winds or expanding hydromagnetic flows that are common in astrophysics, yet we are just beginning to understand the interaction of the solar wind with the interstellar medium in the local arm of the galaxy. This interaction has been a subject of interest for many years [*Davis,* 1955; *Parker,* 1961], but the progress remained slow until 1971, when the situation changed dramatically as a result of clear evidence for the penetration of the neutral interstellar gas into the inner solar system. This evidence was obtained from the Lyman-α sky background measurements from Ogo 5 [*Thomas and Krassa,* 1971; *Bertaux and Blamont,* 1971]. The Lyα sky background was interpreted as resonance scattering of solar 1216-Å radiation from the H atoms in interplanetary space. Reviewing the subject following this discovery, *Axford* [1972] noted that there would be space probes traveling toward the outer regions of the solar system within a few years. Axford was referring to the proposed grand tour opportunities which led to the current Voyager mission. The following decade saw a development of theories of the solar wind–interstellar gas interaction and a series of measurements of Lyα and He (584 Å) sky background from rockets and satellites; a comparison of the theory with the available data has provided information on the direction of motion of the interstellar gas relative to the sun and the density and temperature of the local interstellar medium (for reviews see *Axford* [1972], *Fahr* [1974], *Holzer* [1977], and *Thomas* [1978]). More recently, simultaneous all sky maps in Lyα and He 584 Å were obtained from Mariner 10 [*Broadfoot and Kumar,* 1978; *Ajello,* 1978]. These data show evidence of depletion of solar wind flux at high ecliptic latitudes [*Kumar and Broadfoot,* 1978, 1979]. All of this work relates to observations within 1 AU from the sun well within the ionization cavity around the sun. Since the interaction region extends to 20 AU (or more), data from the outer region of interplanetary space are being obtained by the Voyager UVS. The analysis of this data will improve our understanding of the true nature of the solar wind–interstellar gas interaction.

The Voyager spacecraft are proceeding in an ideal direction for studies of the interstellar medium. The trajectories of the Voyager and Pioneer spacecraft are shown in Figure 29. The ultraviolet photometer aboard Pioneer is body fixed and measures only the outward intensity. The Voyager UV spectrometer can observe the whole celestial sphere. The Pioneer spacecraft have been gathering data for a long time. The Voyager spacecraft are only about a year and a half behind the Pioneer 11 spacecraft, i.e., about 4 AU closer to the sun, and we have the opportunity to cross-calibrate, since the hydrogen and helium column density between us is calculable. This comparison will place the data sets on a common base. The opportunity of obtaining all-sky maps of EUV background in interplanetary space as seen from distances of 1–20 AU from the sun is unlikely to be repeated in the foreseeable future.

One of the most important contributions of the Lyα and He 584 Å sky background measurements is a reliable method of determining the interstellar H and He density just outside the solar system. The densities derived from various spacecraft measurements are listed in Table 3. There is considerable scatter, although the recent measurements favor $N_H = 0.04$ cm^{-3}. In comparison, averages of hydrogen densities to stars at distances of 1–100 pc ranges from 0.003 cm^{-3} to 0.18 cm^{-3} [*Cash et al.,* 1979], which clearly shows that the interstellar medium is clumpy. Evidently, we must rely on the interplanetary EUV background measurements to tell us the true nature of interstellar medium in the neighborhood of the solar system.

The major reason for the disagreement in the estimates of N_H is that the determination of interstellar parameters from the EUV sky background data is model dependent. Typical models of Lyα sky background invoke six parameters to fit the data: (1) the bulk velocity of the interstellar gas relative to the sun, V_b, (2) the temperature of the local interstellar gas T, (3) the density of interstellar hydrogen N_H, (4) resonance scattering efficiency per atom (commonly referred to as the g value), (5) solar radiation pressure on incoming hydrogen atoms parameterized by the dimensionless quantity μ = radiation pressure/solar gravitational force, and (6) hydrogen atom lifetime (τ) or ionization rate, $\beta = 1/\tau$, due to solar wind charge exchange and solar EUV ionization. The Voyager data set will allow us to remove the local interstellar hydrogen and helium densities as variable parameters.

Several maps of Lyα isophotes have been generated from measurements made inside the ionization cavity. A typical example is shown in Figure 30 from the Mariner 10 data [*Broadfoot and Kumar,* 1978]. The same type of plot calculated using nominal parameters derived from the Mariner 10 map, but viewed from Voyager's position at Jupiter, is shown in Figure 31. Figure 32 represents the view from Saturn. The important difference between the Mariner 10 map and the maps from Jupiter and Saturn in Figures 31 and 32 lies in the regions of low intensity. The Mariner 10 map was obtained from inside the emission source function. There is much confusion in the modeling process in the downwind hemisphere of minimum intensity due to the history of the neutral hydrogen passing close to the Sun. In contrast, the low-intensity region observed from the Voyager trajectory will give a good measure of the local interstellar density because the H here has not been subjected to strong solar ionization and the complications of viewing the H column from within the source function are not present. In Figures 31 or 32 the intensity distribution in the outward low-intensity hemisphere is barely sensitive to the downwind cavity which would extend from the sun position to right ascension = 72°. This low-intensity measurement becomes a very stable reference level and will lead to an accurate determination of the hydrogen and helium density.

Multiple scattering is expected to play an important role at $r > 5$ AU [*Keller and Thomas,* 1979]. Our ability to measure both the outward and inward radiation field will provide a first opportunity to address the problem of multiple scattering with pertinent data. The distribution of intensity, as well as the Lyman-α/Lyman-β intensity ratio, will be sensitive to the amount of secondary scattering [cf. *Sandel et al.,* 1978; *Shemansky et al.,* 1979*a*].

Observations from Mariner 10 have already demonstrated that signatures of solar wind structure at high latitudes are clearly observable in the Lyman-α sky background data [*Ku-*

mar and Broadfoot, 1978, 1979]. They also demonstrate other significant departures in the sky background intensity from the predictions of a model assuming spherically symmetric solar wind and solar EUV radiation fields. These results emphasize the importance of a study in three-dimensional space.

The Voyager UVS capability of making simutlaneous measurements of He 584 Å sky background provides important complementary data. The ionization of helium atoms is dominated by solar EUV radiation, and occurs in a region of the heliosphere different from the region of hydrogen ionization, which is due to charge exchange with solar wind protons. Thus the effects of nonuniformities in the three-dimensional structure of solar EUV radiation field on the Lyman-α sky background can be modeled accurately on the basis of the He 584 Å data. The geometry of the observations of the ionization region made from outside the ionization cavity (>5 AU) by the Voyager UVS is well suited for a study of the shape of the ionization cavity and the three-dimensional structure of the heliosphere.

b. *Diffuse Interstellar EUV Radiation Field*

Observations of the interstellar EUV radiation are of interest from several points of view. The galactic component of this radiation field may play an important part in the ionization of the interstellar medium [*Hill and Silk,* 1975]. Furthermore, the discovery and measurement of an extragalactic component would be an important contribution toward dealing with the questions of the existence and characteristics of an intergalactic medium. Predictions of the galactic EUV radiation field have been developed by *Grewing* [1975], *Jura* [1974], *Gondhalekar and Wilson* [1975], and others. Recently, *Henry* [1977] performed integrations of light from catalogued starts to arrive at predictions of the spatial variation of the galactic UV brightness. A useful review of measurements of UV sky brightness has been prepared by *Davidsen et al.* [1974]. This review emphasizes the wide variations in early experimental data. In part, these variations are due to large differences in the size of the field of view of the various instruments used, resulting in varying contributions from hot stars included in the field. With the exception of a recent measurement by *Paresce and Bowyer* [1976], which provided upper limits on the extraterrestrial intensity, no data were available shortward of 1000 Å until our Voyager UVS observations.

The diffuse interstellar EUV spectrum in the wavelength range 750–1200 Å has been measured for the first time with the Voyager ultraviolet spectrometers [*Sandel et al.,* 1979]. Measurements in several directions show intensities at 975 Å ranging from a maximum of about 1×10^{-7} erg cm^{-2} s^{-1} sr^{-1} Å^{-1} to an upper limit of $<1 \times 10^{-8}$ erg cm^{-2} s^{-1} sr^{-1} Å^{-1}.

We have continued to accumulate observations pertinent to this subject. Our preliminary observations have shown that the Voyager interplanetary measurements have an observational threshold one to two orders of magnitude below the near earth upper limits obtained by *Paresce and Bowyer* [1976]. Our measurements show good agreement with the calculations made by *Henry* [1977].

Acknowledgments. The authors would like to acknowledge the assistance of the Voyager Project team at JPL whose tremendous attention to detail make this type of project a success. Within that team, we wish to acknowledge the special assistance of Susan Hanson, James Long, Rick Pomphrey, Charles Stembridge, and Edward Stone. Within the Space Science Institute of U.S.C. we wish to acknowledge the work of Karen DeLay, Bill Ford (deceased), Terry Forrester, Tim McBreen, and useful discussions with Darrell Judge and S. Kumar. This work was supported by the Jet Propulsion Laboratory, California Institute of Technology under NASA contract NAS 7-100. Additional support was provided by the Planetary Sciences Discipline of NASA's Office of Space Sciences.

REFERENCES

Ajello, J., An interpretation of Mariner 10 He (584 Å) and H (1216 Å) interplanetary emission observations, *Astrophys. J., 222,* 1068, 1978.

Allison, A. C., and A. Dalgarno, Band oscillator strengths and transition probabilities for the Lyman and Werner systems of H_2, HD, and D_2. *At. Data, 1,* 289, 1970.

Anderson, R. C., and E. J. Weiler. Copernicus observations of interstellar matter in the direction of HR 1099. *Astrophys. J., 224,* 143, 1978.

Atreya, S. K., and T. M. Donahue, Model ionospheres of Jupiter, in *Jupiter,* edited by T. Gehrels, pp. 304–318, University of Arizona Press, Tucson, 1976.

Atreya, S. K., Y. L. Yung, T. M. Donahue, and E. S. Barker, Search for Jovian auroral hot spots, *Astrophys. J., 218,* L83, 1977.

Atreya, S. K., T. M. Donahue, B. R. Sandel, A. L. Broadfoot, and G. R. Smith. Jovian upper atmospheric temperature measurements by the Voyager 1 UV spectrometer, *Geophys. Res. Lett., 6,* 795, 1979*a*.

Atreya, S. K., T. M. Donahue, and J. H. Waite, Jr., An interpretation of the Voyager measurement of Jovian electron density profiles, *Nature, 280,* 795, 1979*b*.

Atreya, S. K., T. M. Donahue, and M. C. Festou, Jupiter: Structure and composition of the upper atmosphere, submitted to *Astrophys. J. Lett.,* 1981.

Auer, L. H., and H. L. Shipman, A self-consistent model-atmosphere analysis of the EUV white dwarf, HZ-43, *Astrophys. J., 211,* L103, 1977.

Axford, W. I., The interaction of the solar wind with the interstellar medium, in *The Solar Wind, NASA Spec. Publ., 308,* 609, 1972.

Bagenal, F., J. D. Sullivan, and G. L. Siscoe, Spatial distribution of plasma in the Io torus, *Geophys. Res. Lett., 7,* 41, 1980.

Barry, D. C., B. R. Sandel, J. B. Holberg, W. T. Forrester, and A. L. Broadfoot. An upper limit on the EUV flux from HD 192273, *Nature, 285,* 210, 1980.

Bertaux, J. L., and J. E. Blamont, Evidence for a source of an extraterrestrial hydrogen Lyman Alpha emission: The interstellar wind, *Astron. Astrophys., 11,* 200, 1971.

Bertaux, J. L., A. Ammar, and J. E. Blamont, Ogo-5 determination of the local interstellar wind parameters, *Space Res., 12,* 1198, 1972.

Blum, P. W., and H. J. Fahr, Revised interstellar neutral helium/hydrogen density ratios and interstellar UV-radiation field, *Astrophys. Space Sci., 39,* 321, 1976.

Bohlin, R. C., Copernicus observations of interstellar absorption at Lyman-alpha, *Astrophys. J., 200,* 402, 1975.

Bowyer, S., Extreme ultraviolet observations of hot white dwarfs, in *White Dwarfs and Variable Degenerate Stars, IAU Colloq. 53,* edited by H. M. Van Horn and V. Weideman, p. 66, University of Rochester Press, Rochester, N. Y., 1979.

Bridge, H. S., J. W. Belcher, A. J. Lazarus, J. D. Sullivan, R. L. McNutt, F. Bagenal, J. D. Scudder, E. C. Sittler, G. L. Siscoe, V. M. Vasyliunas, C. K. Goertz, and C. M. Yeates, Plasma observations near Jupiter: Initial results from Voyager 1, *Science, 204,* 987, 1979.

Broadfoot, A. L., and S. Kumar, The interstellar wind: Mariner 10 measurements of hydrogen (1216 Å) and helium (584 Å) interplanetary emission, *Astrophys. J., 222,* 1054, 1978.

Broadfoot, A. L., and B. R. Sandel, Self-scanned anode array with a microchannel plate electron multiplier, *Appl. Opt., 16,* 1533, 1977.

Broadfoot, A. L., B. R. Sandel, D. E. Shemansky, S. K. Atreya, T. M. Donahue, H. W. Moos, J. L. Bertaux, J. E. Blamont, J. M. Ajello, D. F. Strobel, J. C. McConnell, A. Dalgarno, R. Goody, M. B. McElroy, and Y. L. Yung, Ultraviolet spectrometer experiment for the Voyager mission. *Space Sci. Rev., 21,* 183, 1977.

Broadfoot, A. L., M. J. S. Belton, P. Z. Takacs, B. R. Sandel, D. E. Shemansky, J. B. Holberg, J. M. Ajello, S. K. Atreya, T. M. Donahue, H. W. Moos, J. L. Bertaux, J. E. Blamont, D. F. Strobel, J. C. McConnell, A. Dalgarno, R. Goody, and M. B. McElroy, Extreme ultraviolet observations from Voyager 1 encounter with Jupiter, *Science, 204,* 979, 1979.

Carlson, R. W., and D. L. Judge, The extreme ultraviolet dayglow of Jupiter, *Planet. Space Sci., 19,* 327, 1971.

Carlson, R. W., and D. L. Judge, Pioneer 10 ultraviolet photometer observations at Jupiter encounter, *J. Geophys. Res., 79,* 3623, 1974.

Carlson, R. W., and D. L. Judge, Pioneer 10 ultraviolet photometer observations of Jupiter: The helium to hydrogen ratio, in *Jupiter,* edited by T. Gehrels, pp. 418–440, University of Arizona Press, Tucson, 1976.

Carlson, R. W., J. C. Bhattacharyya, B. A. Smith, T. V. Johnson, B. Hidayat, S. A. Smith, G. E. Taylor, B. O'Leary, and R. T. Brinkmann, An atmosphere on Ganymede from its occultation of SAO 186800 on 7 June 1972, *Science, 182,* 53, 1973.

Cash, W., S. Bowyer, J. Freeman, M. Lampton, and F. Paresce, Possible detection of an extreme-ultraviolet source at 500 Å, *Astrophys. J., 219,* 585, 1978.

Cash, W., S. Bowyer, and M. Lampton, Interstellar absorption of the extreme ultraviolet flux from two hot white dwarfs, *Astron. Astrophys., 80,* 67, 1979.

Chamberlain, J. W., The excitation of the network nebulae, *Astrophys. J., 117,* 399, 1953.

Clarke, J. T., H. W. Moos, S. K. Atreya, and A. L. Lane, Aurora on Jupiter observed from earth orbit, *Astrophys. J., 241,* L179, 1980.

Cochran, W. D., and E. S. Barker, Variability of Lyman-Alpha emission from Jupiter, *Astrophys. J., 234,* L151, 1979.

Dalgarno, A., and T. L. Stephens, Discrete absorption and photodissociation of molecular hydrogen, *Astrophys. J., 160,* L107, 1970.

Davidsen, A., S. Bowyer, and M. Lampton, Cosmic far ultraviolet background, *Nature, 247,* 513, 1974.

Davis, L., Jr., Interplanetary magnetic fields and cosmic rays, *Phys. Rev., 100,* 1440, 1955.

Dessler, A. J., and J. W. Chamberlain, Jovian longitudinal asymmetry in Io-related and Europa-related auroral hot spots, *Astrophys. J., 230,* 974, 1979.

Dessler, A. J., B. R. Sandel, and S. K. Atreya, The Jovian hydrogen bulge: Evidence for corotating magnetospheric convection, *Planet. Space Sci.,* in press, 1981.

Donnelly, R. F., and J. H. Pope, The 1–3000 Å solar flux for a moderate level of solar activity for use in modeling the ionosphere and upper atmosphere, *NOAA Tech. Rep. ERL 276-SEL 25,* Nat. Oceanic and Atmos. Admin., Rockville, Md., 1973.

Elliott, J. L., L. H. Wasserman, J. Veverka, C. Sagan, and W. Liller, The occultation of Beta Scorpii by Jupiter 2: The hydrogen and helium abundance in the Jovian atmosphere, *Astrophys. J., 190,* 719, 1974.

Eshleman, V. R., G. L. Tyler, G. E. Wood, G. F. Lindal, J. D. Anderson, G. S. Levy, and T. A. Croft, Radio science with Voyager 1 at Jupiter: Preliminary profiles of the atmosphere and ionosphere, *Science, 204,* 976, 1979.

Fahr, H. J., The extraterrestrial UV-background and the nearby interstellar medium, *Space Sci. Rev., 15,* 483, 1974.

Festou, M. C., S. K. Atreya, T. M. Donahue, B. R. Sandel, D. E. Shemansky, and A. L. Broadfoot, Composition and thermal profiles of the Jovian upper atmosphere determined by a Voyager 2 ultraviolet stellar occultation experiment, *J. Geophys. Res., 86,* 5715–5725, 1981.

Fjeldbo, G., A. Kliore, B. Seidel, D. Sweetman, and P. Woiceshyn, The Pioneer 11 radio occultation measurements of the Jovian ionosphere, in *Jupiter,* edited by T. Gehrels, pp. 238–246, University of Arizona Press, Tucson, 1976.

Freeman, J., F. Paresce, S. Bowyer, M. Lampton, R. Stern, and B. Margon, The local interstellar helium density, *Astrophys. J., 215,* L83, 1977.

Freeman, J., F. Paresce, and S. Bowyer, The local interstellar helium density: Corrected, *Astrophys. J., 231,* L37, 1979.

French, R. G., and P. J. Gierasch, Waves in the Jovian upper atmosphere, *J. Atmos. Sci., 31,* 1707, 1974.

Gondhalekar, P. M., and R. Wilson, The interstellar radiation field between 912 Å and 2740 Å, *Astron. Astrophys., 38,* 329, 1975.

Greenstein, J. L., and J. B. Oke, Ultraviolet spectrophotometry of degenerate stars, *Astrophys. J., 229,* L141, 1979.

Grewing, M., The nearby interstellar radiation field between 1750 Å and 504 Å, *Astron. Astrophys., 38,* 391, 1975.

Hanel, R., B. Conrath, M. Flasar, V. Kunde, P. Lowman, W. Maguire, J. Pearl, J. Pirraglia, R. Samuelson, D. Gautier, P. Geirasch, S. Kumar, and C. Ponnamperuma, Infrared observations of the Jovian system from Voyager 1, *Science, 204,* 972, 1979.

Hanel, R. A., B. J. Conrath, L. W. Herath, V. G. Kunde, and J. A. Pirraglia, Albedo, heat, and energy balance of Jupiter: Preliminary results of Voyager infrared investigations, *J. Geophys. Res.,* this issue.

Heise, J., and H. Huizenga, The hot white dwarf HZ-43 II: The helium abundance derived from its ultra-soft X-ray spectrum, *Astron. Astrophys., 84,* 280, 1980.

Henry, R. C., Far ultraviolet studies, I, Predicted far-ultraviolet interstellar radiation field, *Astrophys. J., Suppl., 33,* 451, 1977.

Henry, R. J. W., and M. B. McElroy, The absorption of extreme ultraviolet solar radiation by Jupiter's upper atmosphere, *J. Atmos. Sci., 26,* 912, 1969.

Hill, T. W., Corotation lag in Jupiter's magnetosphere: Comparison of observation and theory, *Science, 207,* 301, 1980.

Hill, J. K., and J. Silk, On the nature of the intercloud medium, *Astrophys. J., 198,* 299, 1975.

Holzer, T. E., Neutral hydrogen in interplanetary space, *Rev. Geophys. Space Phys., 15,* 467, 1977.

Hunt, G. E., and J. P. Muller, Voyager observations of small-scale waves in the equatorial region of the Jovian atmosphere, *Nature, 280,* 778, 1979.

Hunten, D. M., The upper atmosphere of Jupiter, *J. Atmos. Sci., 26,* 826, 1969.

Hunten, D. M., Atmospheres and ionospheres, in *Jupiter,* edited by T. Gehrels, pp. 22–31, University of Arizona Press, Tucson, 1976.

Hunten, D. M., and A. J. Dessler, Soft electrons as a possible heat source for Jupiter's thermosphere, *Planet. Space Sci., 25,* 817, 1977.

Hunten, D. M., and J. Veverka, Stellar and spacecraft occultations by Jupiter: A critical review of derived temperature profiles, in *Jupiter,* edited by T. Gehrels, p. 247, University of Arizona Press, Tucson, 1976.

Johnson, T. V., A. F. Cook II, C. Sagan, and L. A. Soderblom, Volcanic resurfacing rates and implications for volatiles on Io, *Nature, 280,* 746, 1979.

Judge, D. L., R. W. Carlson, F. M. Wu, and U. G. Hartmann, Pioneer 10 and 11 ultraviolet photometer observations of the Jovian satellites, in *Jupiter,* edited by T. Gehrels, p. 1068, University of Arizona Press, Tucson, 1976.

Jura, M., Formation and destruction rates of interstellar H_2, *Astrophys. J., 191,* 375, 1974.

Keller, H. U., and G. E. Thomas, Multiple scattering of solar resonance radiation in the nearby interstellar medium, I, *Astron. Astrophys., 80,* 227, 1979.

Kumar, S., The stability of an SO_2 atmosphere on Io, *Nature, 280,* 758, 1979.

Kumar, S., and A. L. Broadfoot, Evidence from Mariner 10 of solar wind flux depletion at high ecliptic latitudes, *Astron. Astrophys., 69,* L5, 1978.

Kumar, S., and A. L. Broadfoot, Signatures of solar wind latitudinal struture in interplanetary Lyman-α emissions: Mariner 10 observations, *Astrophys. J., 228,* 302, 1979.

Kumar, S., and D. M. Hunten, The atmospheres of Io and other satellites, in *The Satellites of Jupiter,* edited by D. Morrison, University of Arizona Press, Tucson, 1981.

Lampton, M., B. Margon, F. Paresce, R. Stern, and S. Bowyer, Discovery of a non-solar extreme-ultraviolet source, *Astrophys. J., 203,* L71, 1976.

Margon, B., M. Lampton, S. Bowyer, R. Slem, and F. Paresce, An intense extreme-ultraviolet source in Cetus, *Astrophys. J., 210,* L79, 1976.

McClintock, W., R. C. Henry, J. L. Linsky, and H. W. Moos, Ultraviolet observations of cool stars, VI, Local interstellar hydrogen and deuterium Lyman-alpha, *Astrophys. J., 225,* 465, 1978.

McConnell, J. C., B. R. Sandel, and A. L. Broadfoot, Airglow from Jupiter's night side and crescent: Ultraviolet spectrometer observations from Voyager 2, *Icarus, 43,* 128, 1980.

McConnell, J. C., B. R. Sandel, and A. L. Broadfoot, Voyager UV spectrometer observations of He 584 Å dayglow at Jupiter, *Planet. Space Sci.,* in press, 1981.

Meier, R. R., Some optical and kinetic properties of the nearby interstellar gas, *Astron. Astrophys., 55,* 211, 1977.

Mount, G. H., G. L. Rottman, and J. G. Timothy, The solar irradiance 1200–2550 Å at solar maximum, *J. Geophys. Res., 85,* 4271, 1980.

Nagy, A. F., W. L. Chameides, R. H. Chen, and S. K. Atreya, Electron temperatures in the Jovian ionosphere, *J. Geophys. Res., 81,* 5567, 1976.

Orton, G. S., and A. P. Ingersoll, Pioneer 10 and 11 and ground-based infrared data on Jupiter: The thermal structure and He-H_2 ratio, in

Jupiter, edited by T. Gehrels, pp. 206–215, University of Arizona Press, Tucson, 1976.

Paresce, F., and S. Bowyer, Upper limits to the interstellar radiation field between 775, and 1050 Å, *Astrophys. J., 207,* 432, 1976.

Parker, E. N., The stellar-wind regions, *Astrophys. J., 134,* 20, 1961.

Parker, R. A. R., A model for the 'filaments' in the Cygnus Loop, *Astrophys. J., 149,* 363, 1967.

Parsons, S. B., K. G. Henize, J. D. Wray, G. F. Benedict, and M. Laget, Skylab ultraviolet stellar spectra: A new white dwarf, HD 149499 B, *Astrophys. J., 206,* L71, 1976.

Pearl, J., R. Hanel, V. Kunde, W. Maguire, K. Fox, S. Gupta, C. Ponnamperama, and F. Raulin, Identification of gaseous SO_2 and new upper limits for other gases on Io, *Nature, 280,* 755, 1979.

Pilcher, C. B., Images of Jupiter's sulfur ring, *Science, 207,* 181, 1980.

Pilcher, C. B., and D. F. Strobel, Emissions from neutrals and ions in the Jovian magnetosphere, in *The Satellites of Jupiter,* edited by D. Morrison, University of Arizona Press, Tucson, 1981.

Rappaport, S., R. Petre, M. Kayat, K. Evans, G. Smith, and A. Levine, X-ray image of the Cygnus Loop, *Astrophys. J., 227,* 285, 1979.

Raymond, J. C., M. Davis, T. R. Gull, and R. A. R. Parker, Optical detection of a fast shock wave associated with the Cygnus Loop, *Astrophys. J., 238,* L21, 1980*a*.

Raymond, J. C., J. H. Black, A. K. Dupree, L. Hartmann, and R. S. Wolff, Ultraviolet observations of the Cygnus Loop, *Astrophys. J., 238,* 881, 1980*b*.

Sandel, B. R., Azimuthal asymmetry in Io's hot torus, paper presented at the IAU Colloquim 57 on the Satellites of Jupiter, Int. Astron. Union, Kailua-Kona, Hawaii, 1980.

Sandel, B. R., A. L. Broadfoot, and D. E. Shemansky, Microchannel plate life tests, *Appl. Opt., 16,* 1435, 1977.

Sandel, B. R., D. E. Shemansky, and A. L. Broadfoot, Hydrogen Lyβ and Lyα emission lines observed from the interplanetary medium by the Voyager UV spectrometer, *Nature, 274,* 666, 1978.

Sandel, B. R., D. E. Shemansky, A. L. Broadfoot, J. L. Bertaux, J. E. Blamont, M. J. S. Belton, J. M. Ajello, J. B. Holberg, S. K. Atreya, T. M. Donahue, H. W. Moos, D. F. Strobel, J. C. McConnell, A. Dalgarno, R. Goody, M. B. McElroy, and P. Z. Takacs, Extreme ultraviolet observations from Voyager 2 encounter with Jupiter, *Science, 206,* 962, 1979.

Sandel, B. R., A. L. Broadfoot, and D. F. Strobel, Discovery of a longitudinal asymmetry in the hydrogen Lyman-alpha brightness of Jupiter, *Geophys. Res. Lett., 7,* 5, 1980.

Scudder, J. D., E. C. Sittler, and H. S. Bridge, A survey of the plasma electron environment of Jupiter: A view from Voyager, *J. Geophys. Res.,* this issue.

Shemansky, D. E., Radiative cooling efficiencies and predicted spectra of species of the Io plasma torus, *Astrophys. J., 236,* 1043, 1980*a*.

Shemansky, D. E., Mass loading and the diffusive loss rate of the Io plasma torus, *Astrophys. J.,* 1980*b*.

Shemansky, D. E., and G. R. Smith, Voyager 1 EUV spectrum of the Io plasma, submitted to *J. Geophys. Res.,* 1981.

Shemansky, D. E., B. R. Sandel, and A. L. Broadfoot, Voyager observations of the interstellar medium in the 500 to 1700 Å spectral region, *J. Geophys. Res., 84,* 139, 1979*a*.

Shemansky, D. E., B. R. Sandel, and A. L. Broadfoot, Voyager spectral observations of the Cygnus Loop nebula, 600-1700 Å, *Astrophys. J., 231,* 35, 1979*b*.

Shipman, H. L., Spectra of white-dwarf stars at wavelengths < 3000 Å: A theoretical perspective, in *White Dwarfs and Variable Degenerate Stars, IAU Colloq. 53,* edited by H. M. Van Horn and V. Weideman, p. 86, University of Rochester Press, Rochester, N. Y., 1979.

Shipman, H. L., and G. A. Wegner, The high-latitude EUV source HD 192273 as a low-mass binary, *Nature, 281,* 126, 1979.

Srivastava, S. K., and S. Jensen, Experimental differential and integral electron impact cross-sections for the $B^1\Sigma_\mu^+$ state of H_2 in the intermediate-energy region, *J. Phys. B, 10,* 3341, 1977.

Stone, E. J., and E. C. Zipf, Excitation of the Werner bands of H_2 by electron impact, *J. Chem. Phys., 56,* 4646, 1972.

Strobel, D. L., and J. Davis, Properties of the Io plasma torus inferred from Voyager EUV data, *Astrophys. J., 248,* 238, 1980.

Sullivan, J. D., and F. Bagenal, In situ identification of various ionic species in Jupiter's magnetosphere, *Nature, 280,* 798, 1979.

Thomas, G. E., Properties of nearby interstellar hydrogen deduced from Ly-α sky background measurements, in The Solar Wind, *NASA Spec. Publ., 308,* 668, 1972.

Thomas, G. E., The interstellar wind and its influence on the interplanetary environment, *Annu. Rev. Earth Planet. Sci., 6,* 173, 1978.

Thomas, G. E., and R. F. Krassa, Ogo-5 measurements of the Lyman Alpha sky background, *Astron. Astrophys., 11,* 218, 1971.

Thorne, R. M., and B. T. Tsurutani, Diffuse Jovian aurora influenced by plasma injection from Io, *Geophys. Res. Lett., 6,* 649, 1979.

Trafton, L., The Jovian SII torus: its longitudinal asymmetry, *Icarus, 42,* 111, 1980.

Trauger, J. T., G. Munch, and F. L. Roesler, A study of the Jovian SII nebula at high spectral resolution, *Astrophys. J., 236,* 1035, 1980.

Vogt, R. E., W. R. Cook, A. C. Cummings, T. L. Garrard, N. Gehrels, and E. C. Stone, Voyager 1: Energetic ions and electrons in the Jovian magnetosphere, *Science, 204,* 1003, 1979.

Wallace, L., and D. M. Hunten, The Lyman-alpha albedo of Jupiter, *Astrophys. J., 182,* 1013, 1973.

Walter, F., P. Charles, and S. Bowyer, X-ray emission from RS CVn systems: A progress report, *Astrophys. J., 83,* 1539, 1978.

Weller, C. S., and R. R. Meier, Observations of helium in the interplanetary/interstellar wind: The solar-wake effect, *Astrophys. J., 193,* 471, 1974.

Wesselius, P. R., and D. Koester, Effective temperatures of hot white dwarfs, *Astron. Astrophys., 70,* 745, 1978.

Woodgate, B. E., R. P. Kirshner, and R. J. Balon, Radial distribution of Fe XIV emission in the Cygnus Loop, *Astrophys. J., 218,* L129, 1977.

Wray, J. D., S. B. Parsons, and K. G. Henize, HD 149499 B: The hottest white dwarf?, *Astrophys. J., 234,* L187, 1979.

Yung, Y. L., and M. B. McElroy, Stability of an oxygen atmosphere on Ganymede, *Icarus, 30,* 97, 1977.

Yung, Y. L., and D. F. Strobel, Hydrocarbon photochemistry and Lyman-alpha albedo of Jupiter, *Astrophys. J., 239,* 395, 1980.

(Received July 9, 1980;
revised October 17, 1980;
accepted October 17, 1980.)